ACES Asian Chemical Editorial Society

doi.org/10.1002/asia.202100917

CHEMISTRY AN ASIAN JOURNAL Full Paper

Special Collection

Synthesis, Structure and Cytotoxicity of *N,N* and *N,O*-Coordinated Ru^{II} Complexes of 3-Aminobenzoate Schiff Bases against Triple-negative Breast Cancer

Arpan Mukherjee[+], Tuhin Subhra Koley[+], Ayan Chakraborty, Kallol Purkait, and Arindam Mukherjee*[a]

Abstract: Half-sandwich Ru^{II} complexes, $[(YZ)Ru^{II}(\eta^6\text{-arene})(X)]+$, (YZ = chelating bidentate ligand, X = halide), with *N,N* and *N,O* coordination (**1**–**9**) show significant antiproliferative activity against the metastatic triple-negative breast carcinoma (MDA-MB-231). 3-aminobenzoic acid or its methyl ester is used in all the ligands while varying the aldehyde for *N,N* and *N,O* coordination. In the *N,N* coordinated complex the coordinated halide(X) is varied for enhancing stability in solution (X=Cl, I). Rapid aquation and halide exchange of the pyridine analogues, **2** and **3**, in solution are a major bane towards their antiproliferative activity. Presence of free –COOH group (**1** and **4**) make complexes hydrophilic and reduces toxicity. The imidazolyl 3-aminobenzoate based *N,N* coordinated **5** and **6** display better solution stability and efficient antiproliferative activity (IC_{50} ca. 2.3–2.5 μM) compared to the pyridine based **2** and **3** ($IC_{50} > 100$ μM) or the *N,O* coordinated complexes (**7**–**9**) (IC_{50} ca. 7–10 μM). The iodido coordinated, **6**, is resistant towards aquation and halide exchange. The *N,O* coordinated **7**–**9** underwent instantaneous aquation at pH 7.4 generating monoaquated complexes stable for at least 6 h. Complexes **5** and **6**, bind to 9-ethylguanine (9-EtG) showing propensity to interact with DNA bases. The complexes may kill via apoptosis as displayed from the study of **8**. The change in coordination mode and the aldehyde affected the solution stability, antiproliferative activity and mechanistic pathways. The *N,N* coordinated (**5** and **6**) exhibit arrest in the G2/M phase while the *N,O* coordinated **8** showed arrest in the G0/G1 phase.

Introduction

Platinum-based drugs occupy a major share in anticancer chemotherapy, despite the acquired intrinsic resistance in various cancers and major side-effects (viz. nephrotoxicity, neurotoxicity, thrombocytopenia, neutropenia).[1] During the past few decades, there has been significant progress in designing non-platinum (viz. Ru, Ga) anticancer agents.[2–6] The gallium maltolate is in phase-I clinical trial against patients with relapsed glioblastoma (GBM).[7] The Ru^{III} complex NKP-1339 has been in clinical trial against various solid tumors[8–9] and TLD-1433, a Ru^{II} PDT agent, is in Phase I clinical trial against BCG refractory invasive bladder cancer.[10] The promising nature of ruthenium complexes against Pt-drug resistant tumors[11–15] and their lower side effects have spun numerous cytotoxic ruthenium complexes.[11–12,16–35] The pseudo octahedral Ru^{II} complexes can display ligand exchange kinetics similar to Pt^{II} drugs.[36] Ru^{III} complexes display high kinetic inertness and reduce to Ru^{II} in physiology.[37] Half-sandwich piano-stool type Ru^{II} complexes of general formulae $[(YZ)Ru^{II}(\eta^6\text{-arene})(X)]^+$, (YZ = chelating bidentate ligand, X = halide), exhibit significant therapeutic potential against cisplatin-resistant tumor cell lines[3,18,38–46] and several of them viz. RM175, RAPTA-C and RAPTA-T have undergone preclinical trials.[2–3,47–48] Among Ru^{II} complexes, change of the halide leaving group leads to a change in kinetic inertness and alters the mechanism of action in many cases.[49–53] Effect of halide interchange showed remarkable differences in the mechanism of action in certain iminopyridine and azopyridine based ligands and their corresponding $Ru^{II}(\eta^6\text{-}p\text{-cymene})$ complexes.[50,54] The iodido coordinated Ru^{II} complexes show more kinetic inertness and better activity against various forms of cancer including A2780 (ovarian), MCF-7 (breast), HCT116 (colon) and MIA PaCa-2 (pancreatic) cell lines. Certain iodido coordinated Ru^{II} complexes show high potency towards cisplatin-resistant ovarian cancer (A2780cisR), oxaliplatin-resistant colon cancer (HCT116Ox) and p53-null colon cancer (HCT116p53-/−) cells suggesting p53-independent cytotoxicity.[50] Another work showed that chlorido complexes may be internalized in A2780 cells by active transport, while corresponding iodido analogues may follow passive transport.[49] There are examples where the Ru^{II}-iodido complexes are internalized more in cancer cells.[54–55]

Among the various forms of cancer, breast cancer is the second most common cancer in the world and ranks fifth for its fatality.[56] Triple-negative breast cancer (TNBC) is a highly aggressive and metastatic phenotype of breast cancer with a poor prognosis and high relapse rate due to the absence of three major targeting receptors estrogen, progesterone and

[a] *A. Mukherjee,[+] T. S. Koley,[+] A. Chakraborty, Dr. K. Purkait, Dr. A. Mukherjee*
Centre for Advanced Functional Materials (CAFM)
Department of Chemical Sciences
Indian Institute of Science Education and Research Kolkata
Mohanpur-741246 (India)
E-mail: a.mukherjee@iiserkol.ac.in

[+] *These authors contributed equally.*

Supporting information for this article is available on the WWW under https://doi.org/10.1002/asia.202100917

Special Collection *This manuscript is part of a special collection celebrating the 15th Anniversary of IISER Inception.*

HER2.[57] It has been found that p-cymene based Ru^{II} complexes may be an effective choice against triple-negative breast cancer cells.[58–64] In our endeavors, we have generated cytotoxic Ru^{II}-(p-cymene) complexes of imidazole, benzimidazole, anthraimidazoledione and aryl trimethoxy based ligand systems, with excellent efficacy against TNBC,[53,55,65–67] pancreatic cancer,[54] and colon cancer.[65] To gain further insight if the *N,N* vs. *N,O* coordination proceeds with differences in stability and cell killing pathways, we designed nine Ru^{II}(p-cymene) complexes of 3-aminobenzoate while varying the aldehydes (pyridine-2-carboxaldehyde, imidazole-2-carboxaldehyde, salicylaldehyde, 2-hydroxynaphthaldehyde and ortho-vanillin) generating ligands **L1**-**L7**. Among the *N,N* coordinated complexes we also suitably varied the halide (X=Cl, I) to enhance stability and cytotoxicity. Among the above, a Ru^{II} (η^6-benzene) complex of **L1**, which is the Schiff base of pyridine-2-carboxaldehyde and 3-aminobenzoic acid, is reported earlier for biphasic olefin oxidation, although its cytotoxicity is unknown.[68] There is a wide variation in the solution stability and cytotoxicity along with pathways of cell killing among the *N,N* and *N,O* coordinated Ru^{II} (p-cymene) complexes of **L1**–**L7**.

Results and Discussion

The *N,N* donor Schiff base ligands were synthesized from 3-aminobenzoic acid or its methyl ester in condensation with pyridine-2-carboxaldehyde (**L1** and **L2**) and imidazole-2-carboxaldehyde (**L3** and **L4**) in a 1:1 molar ratio. The ligand **L2** was found to dissociate if kept for longer in solution and so the ^{13}C NMR could not be recorded. However, the ^{1}H NMR confirmed formation of **L2** and a quick complexation provided stable complexes **2** and **3** for which the required characterization data are provided. Besides, the **L2** coordinated Ru^{II}-p-cymene complex (**2**) was also characterized by single crystal x-ray crystallography. The *N,O* donor Schiff bases were generated by condensation of the 3-aminobenzoate methyl ester with salicylaldehyde, 2-hydroxynaphthaldehyde and ortho-vanillin (**L5**, **L6** and **L7** respectively). The *N,N* coordinated Ru^{II} (*p*-cymene) complexes (**1** to **6**) were obtained in substantial yields. The coordinated halide was changed to iodido instead of chlorido in certain cases since in the *N,N* coordinated Ru^{II} complexes the iodido coordination is known to affect the cytotoxic efficacies and their pathways.[54] The complexes were synthesized in substantial yields by either refluxing the respective ligands with $[Ru^{II}(p\text{-cymene})X_2]_2$ (X=Cl, I) (**1**–**6**) in methanol for 5–8 h (for *N,N* coordination) or by deprotonating the ligands with KOH, followed by stirring with $[Ru^{II}(p\text{-cymene})Cl_2]_2$ (**7**–**9**) for 24 h, at 25 °C under nitrogen atmosphere (for *N,O* coordination) (Scheme 1). During synthesis of **1**, product was initially obtained as a brown sticky semi-solid with chloride as the counter anion. This sticky mass needed further purification so exchange of the anion with NH_4PF_6 was done in methanol and the solvent evaporated to dryness. Then addition of dichloromethane followed by filtration gave an orange filtrate which on slow evaporation provided orange colored microcrystalline solid of **1**. Complexes **2** and **3** could be isolated with their halide counter anion without any problem so they were not exchanged.

The formula of the complexes are $[Ru^{II}(\mathbf{L1})(p\text{-cymene})X]X$ (X=Cl) (**1**), $[Ru^{II}(\mathbf{L2})(p\text{-cymene})X]X$ (X=Cl, I) (**2**, **3**), $[Ru^{II}(\mathbf{L3})(p\text{-cymene})X]X$ (X=Cl) (**4**), $[Ru^{II}(\mathbf{L4})(p\text{-cymene})X]X$ (X=Cl, I) (**5**, **6**), $[Ru^{II}(\mathbf{L5})(p\text{-cymene})Cl]$ (**7**), $[Ru^{II}(\mathbf{L6})(p\text{-cymene})Cl]$ (**8**) and $[Ru^{II}(\mathbf{L7})(p\text{-cymene})Cl]$ (**9**). Complexes **7**–**9** required purification by flash column chromatography on neutral alumina using 0.1% methanol in dichloromethane as the eluent. All the nine

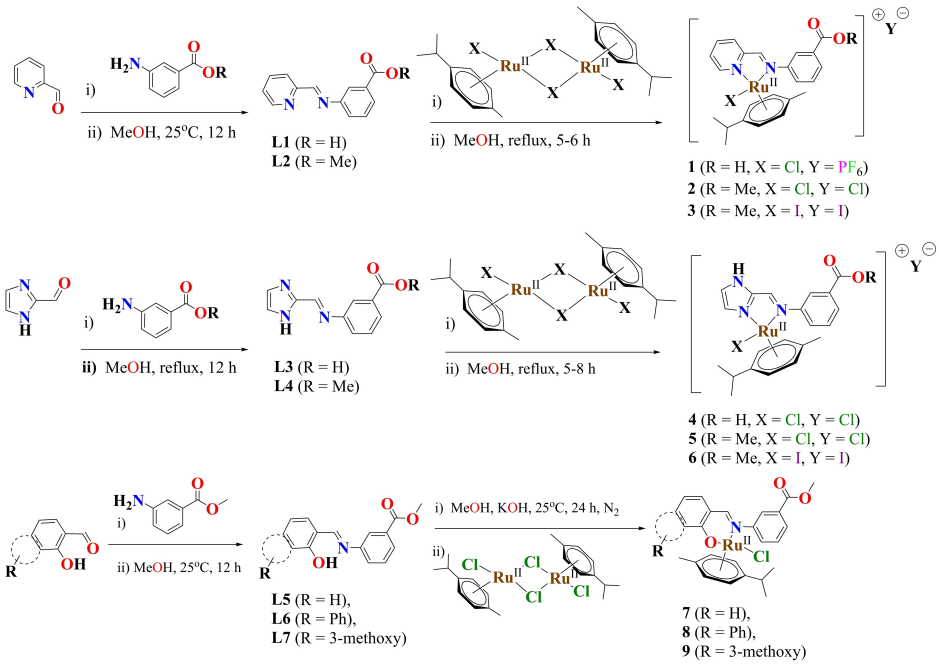

Scheme 1. Representative synthetic scheme of the ligands (**L1** to **L7**) and complexes **1** to **9**.

complexes were well-characterized by ^{1}H & ^{13}C-NMR, ESI-HRMS, UV-Vis and FT-IR (Figures S1–S33). The bulk purity of the complexes was confirmed by elemental analyses.

Complexes (**1**–**9**) exhibited absorption peaks in the ranges 208–251 nm and 284–334 nm corresponding to the π-π* and n-π* transitions respectively. The MLCT transitions appeared as a shoulder in the range 412–453 nm in case of the pyridine-based analogues, **1**–**3** and the three neutral complexes, **7**–**9** (Figures S32, S33). The ^{1}H NMR spectra show that the two methyl groups of the isopropyl moiety in *p*-cymene are not equivalent (Figures S14–S30) after formation of the complexes **2**–**9**. The IR spectra of the complexes depicted the imine (–C=N) bond stretches in the range 1676–1699 cm^{-1}. Complexes **1**–**6** are monocationic in nature and hence, the m/z formulations correspond to $[Ru^{II}$(**L1/L2/L3/L4**)(*p*-cym)(Cl)$]^{+}$ and $[Ru^{II}$(**L2/L4**)(*p*-cym)(I)$]^{+}$ in the ESI-MS positive mode, while they correspond to $[Ru^{II}$(**L5/L6/L7**)(*p*-cym)$]^{+}$ since **7**–**9** are neutral.

X-Ray Crystallography. Good quality single crystals of **2** and **5** were obtained by layering the respective dichloromethane solutions with hexane. The ORTEP diagrams of **2** and **5** are depicted in Figure 1. Complex **2** crystallized in the orthorhombic space group *Pbca* (Table S1), while complex **5** in the monoclinic space group, $P2_1/c$ (Table S1). In each complex, the metal center is in a pseudo tetrahedral arrangement where one vertex is occupied by a chloride, two vertices by the donor atoms of the ligands (*N*,*N* of **L2** and **L4**) and the fourth vertex by the *p*-cymene moiety with a η^6 mode of bonding. Few selected bond distances and angles are provided in Table 1. The distance between the Ru^{II} and the centroid of the *p*-cymene ring is ca. 1.68 Å for **2** and ca. 1.67 Å for **5** suggesting that the *p*-cymene is more tightly bound in the *N*,*N* coordinated 3-aminobenozate based complexes compared to our earlier crystal structures with unsubstituted aniline based schiff base where the distance between the Ru^{II} and the centroid of the *p*-cymene ring was ca. 1.69 Å.[69–70] The lattice chloride balances the resultant mono-positive charge on the metal center in **2** and **5**. The Ru^{II} to imidazole nitrogen bond in **5** is marginally stronger (Ru–N1 ca. 2.072 Å) than the pyridine nitrogen bond in **2** (Ru–N1 ca. 2.099 Å). The structures displayed Ru–Cl bond distances to be ca. 2.40 Å (Table 1). The ∠N1–Ru–N2 in **2** and ∠N1–Ru–N3 in **5** are ca. 76° indicating a distorted tetrahedral structure (Table 1). In complex **2**, the Ru–C15 (ca. 2.199 Å) bond is shorter than the Ru–C18 (ca. 2.2301 Å), although C15 is attached to the bulkier isopropyl group. The same trend is found in **5** (Table 1).

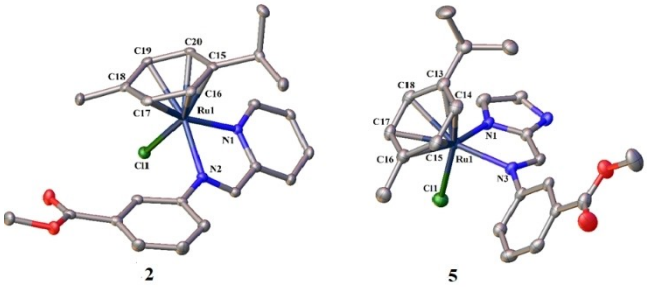

Figure 1. ORTEP diagrams of complexes **2** and **5** with thermal ellipsoids at 50% probability level. The hydrogen atoms and counter-anions are omitted for clarity.

Stability in aqueous buffer solution. The aquation of complexes **1** to **9** were studied in a 3:7 (v/v) DMSO-d_6: 10 mM phosphate buffer (pD = 7.4) containing 4 mM NaCl by ^{1}H-NMR, at different time intervals. The complexes **1** and **4**, having the free carboxylic acid group dissociates in aqueous solution. Complex **1** containing the pyridine bearing **L1** initiates aquation to form the monoaquated adduct (#) within a period of 30 minutes (Figure S34). After 3 h, the complex starts to dissociate to form free **L1** (&) and the dimer $[Ru^{II}_2$(*p*-cymene)$_2Cl_4]$ (@), with subsequent formation of the inactive $[Ru_2$(*p*-cymene)$_2(\mu$-OH)$_3]^{+}$ ($), the latter shows ^{1}H signals at 5.1 and 5.3 ppm,[53,71] (Figure S34). However, even after 24 h there is more than 60% intact complex in solution. We exclude the possibility of DMSO adduct formation since there is no coordinated DMSO peak found in the NMR data in the vicinity of the solvent DMSO peak. Similarly, complex **4** having the imidazole based **L3** and the free pendant carboxylate, underwent gradual aquation from ca. 1 h and after 24 h ca. 50% intact complex was present. The exact specification of the dissociated complex could not be predicted. (Figures S35, S36).

Complexes **2**, **3** and **5**, **6** were probed for their stability in DMSO-d_6 and 10 mM phosphate buffer (3:7 v/v) (pD = 7.4) containing 4 mM NaCl. In addition, the chloride exchange of the iodido analogues (**3** and **6**) were also studied under the same buffer conditions but with 130 mM NaCl. A small amount of the chlorido coordinated **2** ($[Ru^{II}$(**L2**)(*p*-cymene)Cl$]^{+}$) formed the inactive dimer $[Ru_2$(*p*-cymene)$_2(\mu$-OH)$_3]^{+}$ (#), immediately upon dissolution in the 4 mM chloride-containing solution giving rise to the ^{1}H signals at 5.1 and 5.3 ppm.[53,71] The population of the dimer did not increase over 24 h neither any new ^{1}H signal arise (Figure S37) suggesting that the dimer and

Table 1. Selected bond lengths (Å) and bond angles (°) for complexes **2.2H$_2$O** and **5**.

2.2H$_2$O			**5**		
Ru1–Cl1 2.3902(5)	N1–Ru1–N2 76.54(6)	N2–Ru1–Cl1 85.31(5)	Ru1–Cl1 2.4064(8)	N1–Ru1–N3 76.15(10)	N3–Ru1 Cl1 86.48(8)
Ru1–N1 2.099(2)	N1–Ru1–Cl1 86.93(5)	N2–Ru1–C15 116.68 (7)	Ru1–N1 2.072(3)	N1–Ru1–Cl1 85.98(8)	N3–Ru1–C13 118.41(12)
Ru1–N2 2.108(2)	N1–Ru1–C15 93.71(7)	N2–Ru1–C16 94.63 (7)	Ru1–N3 2.104(3)	N1–Ru1–C13 91.52(12)	N3–Ru1–C14 94.58(12)
Ru1–C15 2.199(2)	N1–Ru1–C16 119.69(7)	N2–Ru1–C17 98.85(6)	Ru1–C13 2.181(3)	N1–Ru1–C14 115.48(12)	N3–Ru1–C15 96.42(12)
Ru1–C16 2.180(2)	N1–Ru1–C17 157.42(7)	N2–Ru1–C18 124.96 (6)	Ru1–C14 2.174(3)	N1–Ru1–C15 152.70(12)	N3–Ru1–C16 121.35(12)
Ru1–C17 2.206(2)	N1–Ru1–C18 157.83(7)	N2–Ru1–C19 162.76(7)	Ru1–C15 2.195(3)	N1–Ru1–C16 162.36(12)	N3–Ru1–C17 159.13(12)
Ru1–C18 2.230(2)	N1–Ru1–C19 120.35(6)	N2–Ru1–C20 153.73(7)	Ru1–C16 2.216(4)	N1–Ru1–C17 124.41(12)	N3–Ru1–C18 156.39(13)
Ru1–C19 2.198(2)	N1–Ru1–C20 95.04(7)		Ru1–C17 2.186(3)	N1–Ru1–C18 96.70(12)	
Ru1–C20 2.190(2)			Ru1–C18 2.183(3)		

the original **2** might be in equilibrium under the NMR solution conditions. The corresponding iodido analogue, **3**, is resistant towards hydrolysis up to 24 h in presence 4 mM NaCl (Figure S38). However, in presence of 130 mM chloride, exchange of the coordinated halide initiated upon dissolution and in 24 h, around 50% of the iodido complex **3** exchanged to form the chlorido coordinated **2** (Figure S39).

Complex **5** started to aquate at ca. 1 h in the DMSO-d_6 and 10 mM phosphate buffer (3:7 v/v) (pD = 7.4) containing 4 mM NaCl, followed by gradual dissociation indicating its instability (Figure 2). Aquation for **5** is slow compared to **1**–**4** but it also further dissociates, as visible prominently from 12 h (denoted by '$'). The chemical shifts arising from the dissociated complex do not match with the Ru^{II} dimers or the free **L4**. In the aromatic region, the doublets at 6.16 and 6.05 ppm, corresponding to the mono-aquated **5** decreases with rise in two new doublets at 6.23 and 5.91 ppm, respectively. In a similar fashion, the doublets at 5.69 and 5.38 ppm decrease with rise of new peaks at 5.61 and 5.53 ppm, respectively. Considering the aliphatic region, the mono-aquated **5** gives peaks at 0.96 and 0.57 ppm, corresponding to the $-CH_3$ groups (isopropyl) of the p-cymene ring, the further degraded species of which appear at 0.73 and 0.47 ppm (Figure 2). Thus, the dissociation of **5** leads to complex speciation that could not be characterized with certainty.

In contrast, complex **6**, which is the iodido analogue of **5** is resistant to chloride exchange (ca. 10% of the chlorido complex **5** forms after 24 h) with 130 mM or 4 mM NaCl (Figure 3 and S40). The stacked spectra of both **5** and **6** in presence of DMSO-d_6 and 10 mM phosphate buffer (3:7 v/v) (pD = 7.4) as depicted in Figure 3 (130 mM NaCl) and S40 (4 mM NaCl) supports the above argument. The spectrum showed differences in peak positions and multiplicities, which suggest that **6** is not transformed into **5**. In case of **5**, the proton *ortho*- to the coordinated 'N' in imidazole appears as a singlet and separate from the doublet signal of the proton *ortho*-to the amine of 3-aminobenzoate but *para*- to the carboxylate. In **6** the afore-mentioned proton signals are not distinctly separated from each other (Figure 3, S40). The proton *meta* to the Schiff base nitrogen in the 3-aminonenzoate ring is a doublet in **5** with greater coupling constant, than in **6**. The peak position of the Schiff base proton is shifted from 8.22 in **5**, to 8.34 ppm in **6**. In the aliphatic region, the peak corresponding to the *p*-cymene methyl group is shifted from 2.0 in **5**, to 2.19 ppm in **6**. (Reference to Figure S40 in the supporting info). The above distinct features of **6** are observed to in presence of both 130 mM and 4 mM NaCl condition (Figure 3 and S40 respectively).

The ^{1}H-NMR studies of the aquation of the *N*,*O* coordinated complexes, **7**–**9**, in 3:7 (v/v) DMSO-d_6: 10 mM phosphate buffer (pD = 7.4) containing 4 mM NaCl showed instantaneous mono-aquation, through loss of the chloride. The above result corroborated with the instantaneously monoaquated complex formed using 1.1 equivalents of $AgNO_3$ in a 3:7 (v/v) DMSO-d_6: D_2O mixture (Figure 4, S41, S42, S43). Similar features were observed earlier for other *N*,*O* coordinated Ru^{II}(*p*-cymene) complexes[67,72] suggesting that perhaps the resultant mono-cationic Ru^{II} is a preferred state in aqueous solution at pH 7.4. After hydrolysis, the monoaquated complexes of **7**–**9**, remain stable for ca. 6 h. After this period, the complexes start to dissociate to form the corresponding ligands (#) and free $[Ru^{II}_2(p\text{-cymene})_2Cl_4]$ dimer (@). (Figures S41, S42 and S43).

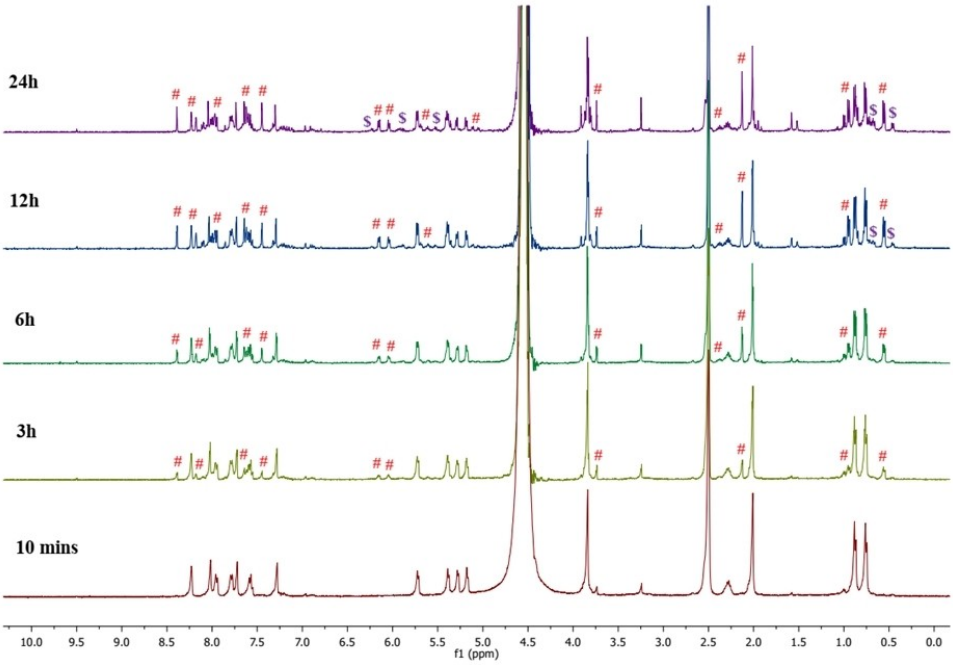

Figure 2. Stability study of **5** in DMSO-d_6 and 10 mM phosphate buffer containing 4 mM NaCl in D_2O (3:7 v/v), (pD = 7.4), monitored by ^{1}H-NMR spectra recorded at 25 °C.'#' stands for aquated species while '$' represents dissociation of the aquated species.

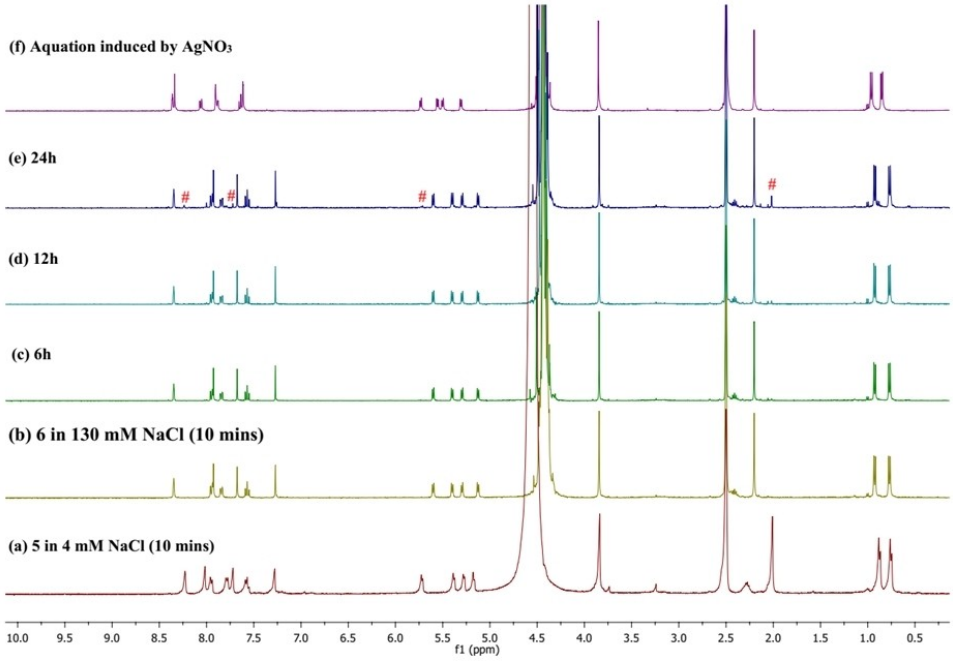

Figure 3. (a) ^{1}H NMR of complex **5** acquired in presence of 3:7 (v/v) DMSO-d_6: 10 mM phosphate buffer solution (pD = 7.4) in D_2O containing 4 mM NaCl (b–e) Chloride exchange study of **6** in DMSO-d_6 and phosphate buffer containing 130 mM NaCl in D_2O (3:7 v/v), (pD = 7.4), monitored by ^{1}H-NMR spectra recorded at 25 °C, at different time intervals, (f) ^{1}H NMR of **6** in presence of (3:7 v/v) DMSO-d_6: D_2O (containing 1.1 equivalents of $AgNO_3$). '#' stands for chloride exchanged species.

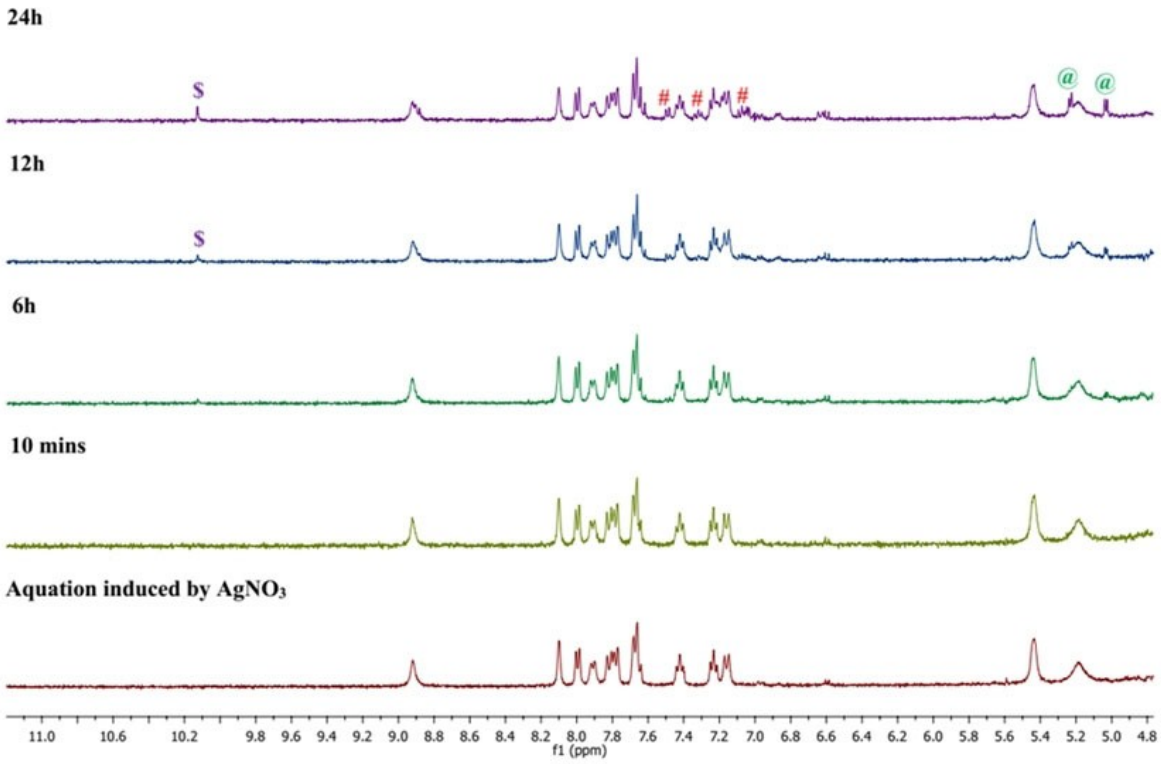

Figure 4. A stack plot of ^{1}H-NMR spectrum to study aquation of complex **8** in 3:7 (v/v) DMSO-d_6: 10 mM phosphate buffer solution (pD = 7.4) containing 4 mM NaCl (aromatic region) at various time intervals in comparison with $AgNO_3$ induced hydrolysis of **8**. '#' represents free ligand; '@' indicates free [Ru^{II}(*p*-cymene)$_2Cl_4$] dimer and '$' corresponds to free aldehyde (–CHO).

Appearance of new doublets in the ranges 5.23–5.25 and 5.02–5.04 ppm were indications of free $[Ru^{II}_2(p\text{-cymene})_2Cl_4]$ dimer formation. The new aliphatic peaks at 1.93 ppm (*p*-cymene methyl) and in the range 1.05–1.09 ppm (*p*-cymene isopropyl) also corroborate the above conclusion. In case of **8**, ligand dissociation was accompanied by simultaneous formation of the constituent aldehyde and amine, as indicated by the appearance of small, but sharp singlet at 10.13 ppm corresponding to free aldehyde (–CHO) (Figure 4).

Binding studies with model nucleobase 9-ethylguanine (9-EtG). Complexes **2** to **6** were investigated for their 9-EtG binding capabilities by means of ^{1}H-NMR, in presence of 3:7 v/v DMSO-d_6: phosphate buffer in D_2O (pD = 7.4) containing 4 mM NaCl and 2 equivalents of 9-EtG. Both **2** and **3** did not undergo any 9-EtG binding for up to 24 h, as no 9-EtG bound peak was observed (Figure S44, S45). However, as mentioned earlier in our aquation studies, **2** exhibited immediate aquation and degradation of the monoaquated species, whereas **3** remained intact. In presence of 9-EtG the ^{1}H-NMR, complex **5** showed aquation and degradation as discussed earlier, and it seems that there is binding of 9-EtG but the singlet of the bound H8 at around 8.02 ppm is merged with the proton ortho to the donor nitrogen in the imidazole of the ligand making it difficult to identify (Figures 5, S46). However, in the ESI-HRMS of **5** bound to the 9-EtG was prominently visible after 12 h (Figure S48–S50) with m/z of 643.1700 (calc. 643.1714), corresponding to the formulation $[Ru^{II}(\mathbf{L4}^-)(p\text{-cym})(9\text{-EtG})]^+$ (Figure S49).

The aqueous solution stable complex **6**, showed poor binding propensity to the model nucleobase 9-EtG and only after 24 h the bound H8 peak in 9-EtG peak was visible in ^{1}H-NMR at 8.02 ppm (denoted by @) (Figures 6, S47). The ESI-HRMS data also supported less affinity to bind with 9-EtG by **6**, in presence 2 equivalents of 9-EtG and only after 24 h the 9-EtG adduct was visible at m/z 643.1695(calc. 643.1714), corresponding to the formulation $[Ru^{II}(\mathbf{L4}^-)(p\text{-cym})(9\text{-EtG})]^+$ (Figure S51–52). The relative intensity of the 9-EtG bound peak of **6** was also lower than the molecular ion peak when compared with **5** after 24 h of incubation (Figures S52, S50). Since both monocationic species are the same after binding, the ionization ability should be the same, thus suggesting that **6** forms lesser amount of 9-EtG adduct compared to **5**. The 9-EtG adduct formation results of **5** and **6** corroborate well with the aquation studies, where **5** slowly converted to its corresponding aquated species under buffer conditions, followed by gradual dissociation (Figure 2) but complex **6** remained intact (Figures 3). Thus, complex **6** is kinetically more inert towards substitution reactions.

Distribution coefficient determination. The cellular uptake and cytotoxic efficacy of Ru^{II} (*p*-cymene) complexes are correlated with their lipophilic behavior.[73] The distribution coefficient (log D) values of complexes **1**–**9** were determined in octanol and 10 mM phosphate buffer solution containing 4 mM NaCl (pH = 7.4). The log D values of the free acid complexes (**1** and **4**) are in the range −0.8 to −1.5, indicating their hydrophilic nature. The quick aquation and chloride exchange of the pyridine analogues (**2** and **3**) as per the ^{1}H-NMR studies, account for their negative lipophilicity values (Figure 7). The imidazole based complexes (**5** and **6**) and the *N,O* coordinated analogues (**7** to **9**) show better lipophilic behaviour with logD values in

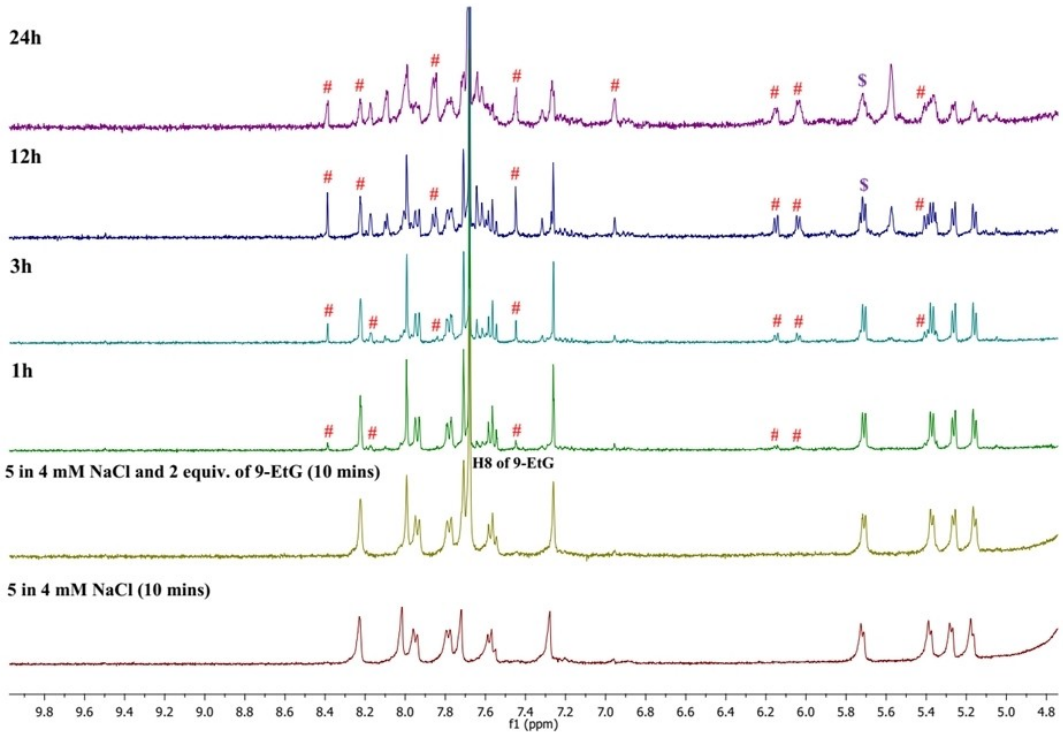

Figure 5. A stack plot of ^{1}H-NMR spectrum to study 9-EtG binding of complex **5** in 3:7 (v/v) DMSO-d_6:10 mM phosphate buffer solution (pD = 7.4) containing 4 mM NaCl and 2-equivalents of 9-EtG. '#' represents aquated species and '$'are the degraded products from the aquated species. Complex **5** without any added 9-EtG under same condition is provided for comparison.

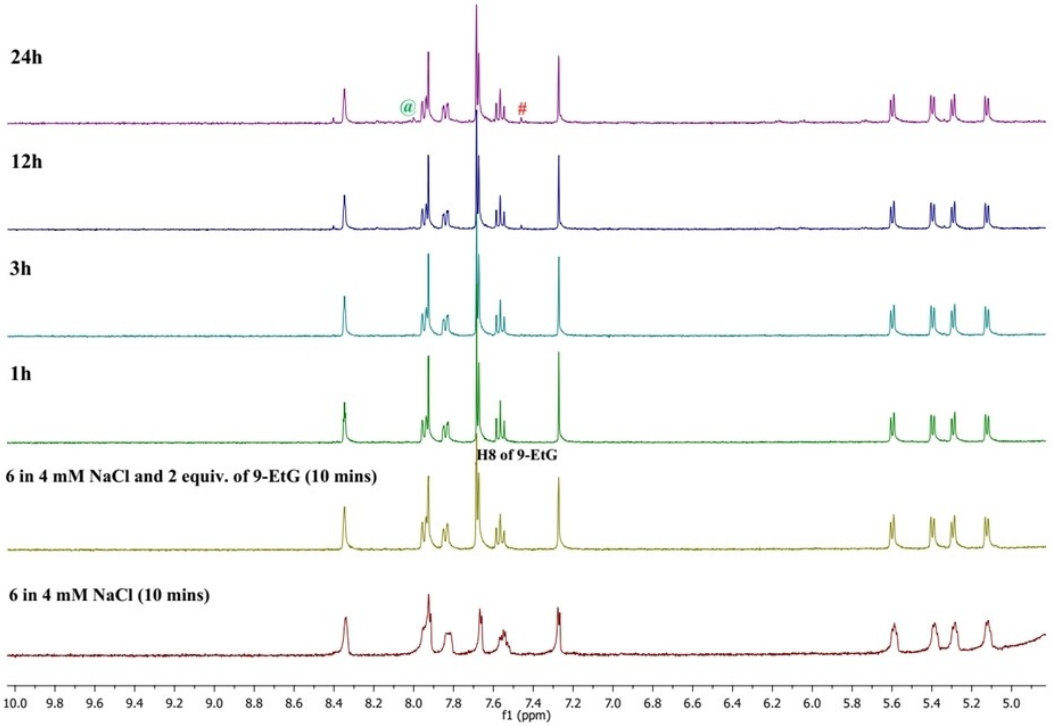

Figure 6. A stack plot of ^{1}H-NMR spectrum to study 9-EtG binding of complex **6** in 3:7 (v/v) DMSO-d_6:10 mM phosphate buffer solution (pD = 7.4) containing 4 mM NaCl and 2-equivalents of 9-EtG. '#' represents chloride exchanged species and '@' represents the 9-EtG bound adduct. Complex **6** without any added 9-EtG under same condition is provided for comparison.

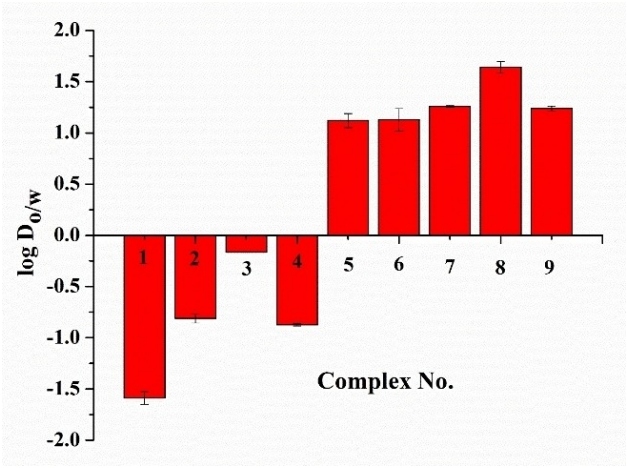

Figure 7. Lipophilicity of the complexes (**1**–**9**) in a 1:1 (v/v) octanol/10 mM phosphate buffer solution containing 4 mM NaCl (pH = 7.4) mixture at 37 °C.

the range of 1.11 ± 0.06 to 1.64 ± 0.05. The lipophilicity values of **5**–**9** correlate well with the cytotoxicity studies performed and discussed later in the cytotoxicity section (Figure 7).

In vitro antiproliferative activity. The complexes were investigated for *in vitro* antiproliferative activity against the metastatic triple-negative breast adenocarcinoma MDA-MB-231 (Table 2, Figure S53–S54). The imidazole-based complexes **5** and **6** displayed significant cytotoxicities (IC_{50} ca. 2.3–2.5 μM) against MDA-MB-231 compared to the corresponding pyridine analogues (**2** and **3**) ($IC_{50} > 100$ μM) as depicted in Table 2 and Figure S53. The complexes, with the free –COOH groups, **1** and **4**, were ineffective, which may be ascribed to their poor solution stability and low pK_a of free acid groups making them difficult to traverse the cell membranes at the physiological pH of 7.4.[65] It may be argued that **1** has PF_6^- as the counter anion and if that is causing the effect.[74] However, **2** has chloride as counter anion and it is also not toxic with a similar ligand thus it is the hydrophilicity and not the PF_6^- counteranion responsible for the poor toxicity of **1**. Complexes **2** and **3** also displayed relatively poor lipophilicity and low antiproliferative activity in spite of esterification of the carboxylic acid. In light of the above aspects, among the *N,N* coordinated Ru^{II} complexes **1**–**6**, the presence of the imidazole motif and esterification of the free acid group, proved to be important in increasing the lipophilicity and antiproliferative efficacy.

The *N,O* coordinated complexes, **7**–**9**, were considerably toxic (IC_{50} ca. 7–10 μM) and the values correlate well with their lipophilic behaviour. Especially, introduction of the 2-hydroxynaphthyl group in **8**, enhanced the lipophilicity and cytotoxicity (ca. 7 μM), as compared to the salicylaldehyde and orthovanillin analogues (ca. 10 μM) (Figure S54). The IC_{50} values of the *N,O* coordinated complexes match well with our previously reported *N,O* coordination bearing ligands in terms of efficacy.[67,75] Thus, esterification and variation of the aldehyde groups, accompanied by change in coordination mode from *N,N* to *N,O*, showed wide variation in cytotoxicity profile against MDA-MB-231. In some previous reports, the switch of coordination mode from *N,N* to *N,O* resulted in increased efficacy.[76–77]

Table 2. IC_{50}(μM) ± S.D values of complexes **1**–**9** against triple negative breast carcinoma (MDA-MB-231) (S.D. = Standard Deviation).

IC_{50} ± SD(μM)[a] Complexes	MDA MB-231	Complexes	MDA MB-231
1	> 100	**6**	2.3 ± 0.2
2	> 100	**7**	10.1 ± 0.1
3	> 100	**8**	7.1 ± 0.7
4	> 100	**9**	10.6 ± 0.7
5	2.5 ± 0.3	oxaliplatin	19.3 ± 1.2

[a] IC_{50} values were calculated by non-linear curve fitting in dose response inhibition-variable slope model using graph pad prism. Data presented are mean of three independent experiments, in a single experiment each concentration was assayed in triplicate. The statistical significance (p) of the data is < 0.05 or better.

For instance, in a series of Ru^{II} (*p*-cymene) complexes of iminophosphorane ligands the *N,O* coordinated analogues were appreciably more toxic against a series of investigated cell lines (IC_{50} ca. 1.5–9.9 μM), than their *N,N* counterparts (IC_{50} ca. 6.6–148 μM).[77] In another study, a *N,O* coordinated antipyrine based Ru^{II} (*p*-cymene) complex exhibited significant activity against K562 (chronic myolegenous leukemia) (IC_{50} ca. 12 μM), while the corresponding *N,N* coordinated analogue was moderately active (IC_{50} ca. 60 μM).[76] They also revealed that salicylaldehyde based Ru^{II} (*p*-cymene) complexes (*N,O*) are more potent than the corresponding pyridine-2-carboxaldehyde (*N,N*) based complexes[76] which is similar to our results presented herein. Interestingly, as already mentioned above, our studies suggest that the cytotoxic potential improves in *N,N* coordinated complexes compared to their neutral *N,O* counterparts when the imidazole motif is present in the former. Thus, we show that proper ligand choice render *N,N* coordinated Ru^{II} (*p*-cymene) complexes ca. 3–4 times more cytotoxic than *N,O* coordinated analogues. Further investigation shows that the change of *N,N* to *N,O* coordination also changes the cell-killing pathway.

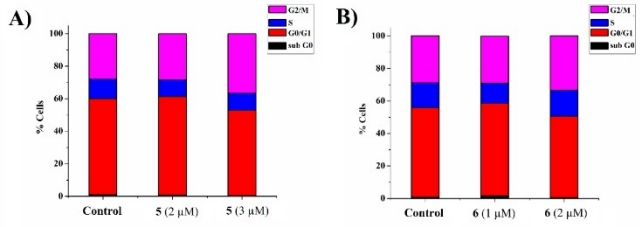

Figure 8. Cell cycle analyses of complexes **5** (3 and 2 μM) and **6** (2 and 1 μM) showing G2/M phase arrest in MDA-MB-231.

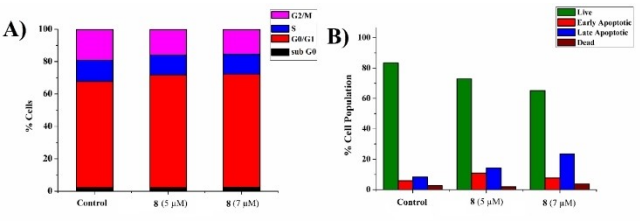

Figure 9. *In vitro* mechanistic studies of complex **8** against MDA-MB-231 using flow cytometry. (**A**) Cell cycle arrest incurred in MDA-MB-231 cells using 5 and 7 μM concentrations for 18 h. and (**B**) Induction of apoptosis by 5 and 7 μM concentrations in a dose-dependent manner.

Pathways of cell killing. Flow cytometry investigations of the *N,N* coordinated complexes **5** (3 and 2 μM doses) and **6** (2 and 1 μM doses), for their effects on cell cycle in MDA-MB-231, show arrest at the G2/M phase, suggesting the chlorido to iodido coordination did not change the pathway of cell killing in a major fashion (Figure 8, S55, S56). On the other hand, the *N,O* coordinated complex **8** exhibited cycle arrest in the G0/G1 phase (Figure 9, S57). Hence, a clear difference in mechanism of action was established upon change in coordination mode. Change in cell cycle arrest pathway upon coordination environment alteration, as presented herein is also a distinctive proof of the designed complexes following different action pathways. In the G1 phase, the cells synthesize various mRNA's and proteins for proper replication of DNA in the S phase.[78] Hence, **8** may be interfering with similar processes which consequently hindered the cell cycle progression to the S phase (Figure S57). The literature studies show that *N,O* coordinated Ru^{II} (*p*-cymene) complexes may manage to evade apoptosis upon caspase inhibition in Jurkat cells, while its corresponding *N,N* partner did not display any such effect, i.e, caspase inhibition did not prevent cell death or apoptosis.[77] In our case we observe change in the phase of cell cycle arrest upon coordination environment alteration from *N,N* and *N,O*. Thus providing a distinctive proof of the coordinated complexes following different action pathways. Annexin V-PE/7-AAD double staining assay using two different dosages of **8** (5 and 7 μM) showed that there was ca. 11% and 18% apoptosis respectively, after treatment for 18 h (Figure 9, S58). The percentage of the late apoptotic population increased with increase in dose, where the cells become stained with both Annexin-V and 7-AAD. The results suggest that complexes may be killing via apoptosis.

Conclusion

We have synthesized and characterized a series of *N,O* and *N,N*-coordinated Ru^{II} complexes (**1**–**9**) with ligands having 3-aminobenzoate forming Schiff bases with five different aldehydes. Similar to our earlier reports,[65] the pyridine based *N,N*-coordinated complexes are less stable, more hydrophilic and less cytotoxic (**1**–**4**). The presence of a pendant free carboxylic acid group also decreased cytotoxicity (**1** and **4**). The imidazole donor based *N,N* chelated iodido coordinated Ru^{II}-(*p*-cymene) complex is the most stable but unless they are sufficiently lipophilic they are not cytotoxic as evident from differences in **3** and **6**. The *N,O* coordinated Ru^{II}-(*p*-cymene) complexes aquate rapidly and the mono-aquated species remain stable in physiological condition for ca. 6 h before initiating dissociation but even after 24 h around 60% of the complexes are intact. Among the *N,O* coordinated Ru^{II}-(*p*-cymene) complex, the 2-hydroxynapthyl and 3-aminobenzoate based **8** exhibits maximum antiproliferative activity but it is still three times less toxic than the *N,N* coordinated, imidazolyl and 3-aminobenzoate

based **5** and **6**. DNA seems to be a potential target for the complexes since binding to the model DNA base 9-ethylguanine is observed. The most antiproliferative complex **6** is ca. 8 times more active than oxaliplatin against MDA-MB-231. Complex **8** kills via apoptosis. The change in *N,N* to *N,O* coordination due to the alteration of the aldehyde alters the response to cell cycle arrest, with the imidazole based *N,N* chelated **5** and **6** arresting the G2/M phase, whereas the 2-hydroxynaphthyl based *N,O* chelated **8** arrests the G0/G1 phase.

Experimental Section

Materials and methods. All chemicals and solvents were purchased from commercial sources. Solvents were distilled and dried prior to use by standard procedures.[79] Pyridine 2-carboxaldehyde, imidazole-2-carboxaldehyde, salicylaldehyde, ortho-vanillin and 2-hydroxynaphthaldehyde were purchased from Sigma Aldrich and used without any further purification. 3-aminobenzoic acid was purchased from Spectrochem, India. Ruthenium (III) trichloride was purchased from Precious Metals Online, Australia. $[Ru^{II}(\eta^6\text{-}p\text{-cymene})Cl_2]_2$ was prepared using a literature protocol.[80] 9-ethyl guanine (9-EtG) was purchased from Sigma Aldrich and used for binding experiments as received. MTT [3-(4,5-dimethylthiazol-2-yl)-2,5-diphenyltetrazolium bromide] (USB), along with supplements and assay kits were purchased from Gibco and used as received. UV-visible measurements were done using an Agilent Cary 300 UV-vis spectrophotometer. FT-IR spectra were recorded via Perkin-Elmer SPECTRUM RX I spectrometer using ATR probe. ^{1}H & proton decoupled ^{1}H decoupled ^{13}C NMR spectra were measured using either JEOL ECS 400 MHz or Bruker Avance III 500 MHz spectrometer at room temperature. The chemical shifts are reported in parts per million (ppm). Electrospray ionization mass spectra were recorded using a Bruker maXis II mass spectrometer by positive mode of electrospray ionization. Elemental analyses were performed using a Perkin-Elmer 2400 series II CHNS/O analyzer. The synthetic yields reported are of isolated analytically pure compounds. The ligands and complexes synthesized were dried in vacuum and stored in a desiccator in dark.

Syntheses

Synthesis of (E)-3-(pyridin-2-ylmethyleneamino)benzoic acid (L1). To a stirred solution of 3-aminobenzoic acid (0.1 g, 0.729 mmol) in methanol, pyridine-2-carboxaldehyde (0.078 g, 0.729 mmol), was added dropwise, under ice-cold conditions. The whole mixture was allowed to stir for 12 h at 25 °C under nitrogen atmosphere. The solvent was evaporated under reduced pressure and the yellowish-white crude was washed twice with diethyl ether, followed by cold hexane. Product was isolated as a white fluffy powder, with a yellow tinge, after drying in vacuum. Yield: 0.140 g (85%). ^{1}H NMR (400 MHz, DMSO-d_6): δ 8.75 (d, 1H, J = 4.6 Hz, Py–H), 8.63 (s, 1H, –CH=N), 8.19 (d, 1H, J = 7.92 Hz, Py–H), 8.00 (m, 1H, Py–H), 7.88 (m, 1H, Py–H), 7.81 (s, 1H, Ar–H), 7.59 (m, 3H, Ar–H), 13.09 (br.s, 1H, –COOH–) (Figure S1). ^{13}C NMR (125 MHz, DMSO-d_6) δ 167.49, 162.48, 154.30, 151.24, 150.26, 137.63, 132.53, 130.20, 127.90, 126.37, 125.82, 122.42, 121.99 (Figure S2).

Synthesis of methyl (E)-3-((pyridine-2-ylmethylene)amino) benzoate (L2): To a stirred solution of methyl-3-aminobenzoate (0.1 g, 0.661 mmol) in methanol, pyridine-2-carboxaldehyde (0.070 g, 0.661 mmol), was added dropwise, under ice-cold conditions. The whole mixture was allowed to stir for 12 h at 25 °C under nitrogen atmosphere. The solvent was evaporated under reduced pressure and the off-white crude was washed two times with diethyl ether, followed by petroleum ether. Product was isolated as a white sticky semi-solid, with a light brown tinge, after drying in vacuum. The product quickly dissociates in solution and hence ^{13}C spectrum over long scans could not be recorded. Due to this reason, the isolated crude was reacted immediately with the metal precursor. Yield: 0.112 g (71%). ^{1}H NMR (500 MHz, DMSO-d_6): δ 8.75 (d, 1H, J = 4.2 Hz, Py–H), 8.63 (s, 1H, –CH=N), 8.19 (d, 1H, J = 7.85 Hz, Py–H), 8.00 (t, 1H, J = 7.7 Hz, Py–H), 7.89 (d, 1H, J = 7.07 Hz, Py–H), 7.83 (s, 1H, Ar–H), 7.62 (m, 3H, Ar–H), 3.88 (s, 3H, –COOMe) (Figure S3).

Synthesis of (E)-3-(((1H-imidazol-2-yl)methylene)amino)benzoic acid (L3). To a stirred solution of 3-aminobenzoic acid (0.1 g, 0.729 mmol) in methanol, imidazole-2-carboxaldehyde (0.070 g, 0.729 mmol), was added dropwise. The whole mixture was allowed to reflux for 12 h. The solvent was evaporated under reduced pressure and the off-white crude was washed two times with diethyl ether. Product was isolated as a yellowish-white solid after drying in vacuum. Yield: 0.137 g (87%). ^{1}H NMR (500 MHz, DMSO-d_6): δ 13.11 (br.s, 1H, –NH), 8.44 (s, 1H, –CH=N), 7.84 (m, 1H, Ar–H), 7.77 (s, 1H, Ar–H), 7.55 (m, 2H, Ar–H), 7.37 (s, 1H, Imi-H),7.21 (s, 1H, Imi-H) (Figure S4).^{13}C NMR (125 MHz, DMSO-d_6) δ 167.55, 151.97, 151.49, 145.25, 132.55, 130.20, 127.40, 125.61, 122.38 (Figure S5).

Synthesis of methyl (E)-3-(((1H-imidazol-2-yl)methylene)amino) benzoate (L4). To a stirred solution of methyl-3-aminobenzoate (0.1 g, 0.661 mmol) in methanol, imidazole-2-carboxaldehyde (0.063 g, 0.661 mmol), was added dropwise. The whole mixture was allowed to reflux for 12 h. The solvent was evaporated under reduced pressure and the off-white crude was washed twice with diethyl ether. Product was isolated as a yellowish-white solid after drying in vacuum. Yield: 0.125 g (83%). ^{1}H NMR (500 MHz, DMSO-d_6): δ 13.13 (br.s, 1H, –NH), 8.45 (s, 1H, –CH=N), 7.85 (m, 1H, Ar–H), 7.79 (s, 1H, Ar–H), 7.59 (m, 2H, Ar–H), 7.30 (br.s, 2H, Imi-H), 3.88 (s, 3H, –COOMe) (Figure S6). ^{13}C NMR (125 MHz, DMSO-d_6) δ 166.43, 152.12, 151.53, 145.18, 131.25, 130.35, 127.13, 126.01, 122.21, 52.76 (Figure S7).

Synthesis of methyl (E)-3-((2-hydroxybenzylidene)amino) benzoate (L5). To a stirred solution of methyl-3-aminobenzoate (0.2 g, 1.323 mmol) in methanol, salicylaldehyde (0.161 g, 1.323 mmol) was added dropwise over a period of 15 mins. The resulting solution was allowed to stir at 25 °C for 12 h under nitrogen atmosphere. The solvent was evaporated under reduced pressure and the obtained crude product was washed twice with petroleum ether, yielding a deep yellow solid. Yield: 0.238 g (81%). ^{1}H NMR (500 MHz, $CDCl_3$): δ 8.68 (s, 1H, –CH=N), 7.97 (m, 2H, Sal-H), 7.51 (d, 2H, J = 5.1 Hz, Sal-H and Ar–H), 7.45 (dd, 2H, Ar–H), 7.12 (d, 1H, J = 8.3 Hz, Sal-H), 6.98 (t, 1H, J = 7.4 Hz, Sal-H), 3.94 (s, 3H, –OCH_3) (Figure S8). ^{13}C NMR (125 MHz, DMSO-d_6, 25 °C): δ 166.39, 165.09, 160.77, 149.19, 134.15, 133.19, 131.45, 130.51, 127.87, 126.94, 122.18, 119.82, 119.76, 117.16, 52.86 (Figure S9).

Synthesis of methyl (E)-3-(((1-hydroxynaphthalen-2-yl)methylene) amino)benzoate (L6). To a stirred solution of methyl-3-aminobenzoate (0.2 g, 1.323 mmol) in methanol, 2-hydroxynaphthaldehyde (0.227 g, 1.323 mmol) was added dropwise to the above solution and allowed to stir at 25 °C for 12 h under nitrogen atmosphere. The solvent was evaporated under reduced pressure and the obtained crude was washed repeatedly with petroleum ether, yielding a bright yellow solid. Yield: 0.298 (74%). ^{1}H NMR (500 MHz, DMSO-d_6): δ 10.82 (s, 1H, Naph-OH), 9.74 (d, 1H, J = 4.2 Hz, –CH=N), 8.56 (d, 1H, J = 8.4 Hz, Naph-H), 8.09 (t, 1H, Ar–H), 7.98 (d, 1H, J = 9.2 Hz, Naph-H), 7.94 (m, 1H, Ar–H), 7.89 (m, 1H, Ar–H), 7.83 (d, 1H, J = 7.6 Hz, Naph-H), 7.67 (t, 1H, J = 7.9 Hz, Naph-H), 7.57 (m, 1H, Ar–H), 7.39 (dd, 1H, Naph-H), 7.07 (t, 1H, J = 9.2 Hz, Naph-H), 3.91 (s, 3H, –OCH_3) (Figure S10). ^{13}C NMR (125 MHz, DMSO-d_6, 25 °C): δ 169.26, 165.84, 157.33, 145.07, 136.92, 133.03,

131.06, 130.05, 128.98, 128.11, 126.91, 126.84, 125.27, 123.63, 121.59, 121.39, 120.64, 108.81, 52.35 (Figure S11).

Synthesis of methyl (E)-3-((2-hydroxy-3-methoxybenzylidene) amino)benzoate (L7). To a stirred solution of methyl-3-amino-benzoate (0.2 g, 1.323 mmol) in methanol, ortho-vanillin (0.201 g, 1.323 mmol) was added dropwise to the above solution and allowed to stir at 25 °C for 12 h under nitrogen atmosphere. The solvent was evaporated under reduced pressure and the obtained crude was washed repeatedly with petroleum ether, yielding a yellow solid. Yield: 0.320 g (83%). ^{1}H NMR (500 MHz, DMSO-d_6): δ 12.88 (s, 1H, Van-OH), 9.03 (s, 1H, –CH=N), 7.93 (m, 2H, Ar–H), 7.71 (m, 1H, Ar–H), 7.64 (t, 1H, J = 7.8 Hz, Ar–H), 7.31 (dd, 1H, Van-H), 7.17 (dd, 1H, Van-H), 6.95 (t, 1H, J = 7.9 Hz, Van-H), 3.89 (s, 3H, Van-OCH_3), 3.83 (s, 3H, –OCH_3) (Figure S12). ^{13}C NMR (125 MHz, DMSO-d_6, 25 °C): δ 165.85, 164.71, 150.46, 148.49, 147.91, 130.93, 129.99, 127.36, 126.36, 123.95, 121.65, 119.23, 118.72, 115.80, 55.88, 52.32 (Figure S13).

[(L1)Ru^{II}(η^6-p-cym)Cl](PF$_6$) (1). To a stirred solution of **L1** (0.08 g, 0.353 mmol) in methanol, [Ru^{II}(η^6-p-cymene)Cl$_2$]$_2$ (0.108 g, 0.176 mmol) was added dropwise and allowed to reflux for 5 h. The entire solution was cooled to room temperature followed by which, NH_4PF_6 (0.069 g, 0.42 mmol) was added and stirred for 1 h. The solvent was evaporated under reduced pressure. The yellow crude was re-dissolved in dichloromethane, filtered and re-evaporated. The orange crude was washed two times with diethyl ether, yielding an orange solid, which was dried in vacuum. Yield: 0.171 g (72%). Anal. Calcd for $C_{23}H_{24}ClF_6N_2O_2PRu$: C, 43.03; H, 3.77; N, 4.36. Found C, 42.79; H, 3.75; N, 4.42. ^{1}H NMR (500 MHz, DMSO-d_6): δ 13.41 (br.s, 1H, –COOH), 9.59 (d, 1H, J = 5.6 Hz, Py–H), 8.99 (s, 1H, –CH=N), 8.36 (m, 3H, Ar–H), 8.14 (d, 1H, J = 7.7 Hz, Py–H), 8.07 (d, 1H, J = 7.9 Hz, Ar–H), 7.92 (t, 1H, J = 6.6 Hz, Py–H), 7.79 (t, 1H, J = 7.9 Hz, Py–H), 6.07 (d, 1H, J = 6.3 Hz, p-cym-H), 5.78 (d, 1H, J = 6.3 Hz, p-cym-H), 5.71 (d, 1H, J = 6.0 Hz, p-cym-H), 5.52 (d, 1H, J = 6.1 Hz, p-cym-H), 2.53 (m, 1H, p-cym-CH), 2.16 (s, 3H, p-cym-CH_3), 1.01 (d, 3H, J = 6.9 Hz, iPr–CH_3), 0.97 (d, 3H, J = 6.8 Hz, iPr–CH_3) (Figure S14). ^{13}C NMR (125 MHz, DMSO-d_6) δ 168.63, 166.39, 155.98, 154.50, 151.77, 139.96, 132.09, 130.30, 130.27, 129.96, 129.06, 126.82,123.08, 105.44, 102.97, 86.75, 85.57, 85.17, 85.11, 52.56, 30.42, 21.87, 21.83, 18.17 (Figure S15). UV-vis.: [CH_3OH, λ_{max}, nm(ε/dm^{3}mol^{-1}cm^{-1})]: 211 (8040), 307 (2510), 422 (740) (Figure S32). FT-IR (cm^{-1}): 3701, 2983, 1683, 1526, 1441, 1221, 809, 759, 674. ESI-HRMS (Methanol) m/z (calc): 497.0568 (497.0564) [$C_{23}H_{24}ClN_2O_2Ru^+$].

[(L2)Ru^{II}(η^6-p-cym)Cl]Cl (2). To a stirred solution of **L2** (0.1 g, 0.416 mmol) in methanol, [Ru^{II}(η^6-p-cymene)Cl$_2$]$_2$ (0.127 g, 0.208 mmol) was added dropwise and allowed to reflux for 5 h. The solvent was evaporated under reduced pressure. The reddish-orange crude was washed two times with diethyl ether, yielding a deep orange solid, which was dried in vacuum. Yield: 0.116 g (51%). Anal. Calcd for $C_{24}H_{26}Cl_2N_2O_2Ru$: C, 52.75; H, 4.80; N, 5.13. Found C, 52.58; H, 4.77; N, 5.17. ^{1}H NMR (500 MHz, DMSO-d_6): δ 9.63 (d, 1H, J = 5.4 Hz, Py–H), 9.04 (s, 1H, –CH=N), 8.39 (s, 1H, Ar–H), 8.34 (m, 2H, Py–H), 8.16 (d, 1H, J = 7.6 Hz, Py–H), 8.12 (d, 1H, J = 7.9 Hz, Ar–H), 7.92 (t, 1H, J = 6.1 Hz, Ar–H),7.82 (t, 1H, J = 7.8 Hz, Ar–H), 6.09 (d, 1H, J = 6.2 Hz, p-cym-H), 5.80 (d, 1H, J = 5.9 Hz, p-cym-H), 5.73 (d, 1H, J = 6.0 Hz, p-cym-H), 5.55 (d, 1H, J = 6.0 Hz, p-cym-H), 3.94 (s, 3H, –COOMe), 2.16 (s, 3H, p-cym-CH_3), 1.01 (d, 3H, J = 6.9 Hz, iPr–CH_3), 0.97 (d, 3H, J = 6.8 Hz,iPr–CH_3) (Figure S16). ^{13}C NMR (125 MHz, DMSO-d_6) δ 169.03, 165.35, 156.06, 154.50, 151.82, 139.96, 130.82, 130.38, 130.17, 130.09, 129.10, 127.23, 123.00, 105.60, 102.82, 86.73, 85.74, 85.18, 84.91, 52.57, 30.42, 21.86, 21.35, 18.14 (Figure S17). UV-vis.: [CH_3OH, λ_{max}, nm(ε/dm^{3}mol^{-1}cm^{-1})]: 208 (10160), 302 (2810), 422 (1490) (Figure S32). FT-IR (cm^{-1}): 3335, 2926, 1700, 1427, 1270, 1086, 972, 745. ESI-HRMS (Methanol) m/z (calc): 511.0721 (511.0721) [$C_{24}H_{26}ClN_2O_2Ru^+$].

[(L2)Ru^{II}(η^6-p-cym)(I)]I (3). To a stirred solution of **L2** (0.1 g, 0.416 mmol) in methanol, [Ru^{II}(η^6-p-cymene)I$_2$]$_2$ (0.203 g, 0.208 mmol) was added dropwise and allowed to reflux for 6 h. The solvent was evaporated under reduced pressure. The brownish-orange crude was washed two times with diethyl ether, yielding an orange solid, with a deep brown tinge. The product was dried in vacuum. Yield: 0.230 g (77%). Anal. Calcd for $C_{24}H_{26}I_2N_2O_2Ru$: C, 39.52; H, 3.59; N, 3.84. Found C, 39.75; H, 3.55; N, 3.89. ^{1}H NMR (500 MHz, DMSO-d_6): δ 9.59 (d, 1H, J = 5.5 Hz, Py–H), 8.96 (s, 1H, –CH=N), 8.46 (s, 1H, Ar–H), 8.34 (dt, 2H, Py–H), 8.19 (dd, 2H, Py–H), 7.88 (t, 1H, J = 7.3 Hz, Ar–H), 7.81 (t, 1H, J = 7.9 Hz, Ar–H), 5.98 (d, 1H, J = 6.3 Hz, p-cym-H), 5.85 (d, 1H, J = 6.2 Hz, p-cym-H), 5.77 (d, 1H, J = 6.1 Hz, p-cym-H), 5.55 (d, 1H, J = 6.2 Hz, p-cym-H), 3.94 (s, 3H, –COOMe), 2.65 (m, 1H, p-cym-CH), 2.36 (s, 3H, p-cym-CH_3), 1.03 (d, 3H, J = 6.9 Hz, iPr–CH_3), 0.95 (d, 3H, J = 6.9 Hz, iPr–CH_3) (Figure S18). ^{13}C NMR (125 MHz, DMSO-d_6) δ 168.67, 165.28, 157.30, 154.47, 152.29, 139.61, 130.78, 130.55, 130.26, 130.09, 128.59, 127.85, 123.64, 107.97, 101.25, 87.10, 86.21, 86.00, 84.80, 52.56, 30.91, 21.88, 21.26, 19.59 (Figure S19). UV-vis.: [CH_3OH, λ_{max}, nm(ε/dm^{3}mol^{-1}cm^{-1})]: 220 (9450), 300 (2300), 453 (440) (Figure S32). FT-IR (cm-1): 3701, 3566, 2926, 1694, 1519, 1441, 1256, 1164, 1086, 972, 752. ESI-HRMS (Methanol) m/z (calc): 603.0074 (603.0077) [$C_{24}H_{26}IN_2O_2Ru^+$].

[(L3)Ru^{II}(η^6-p-cym)Cl]Cl (4). To a stirred solution of **L3** (0.1 g, 0.464 mmol) in methanol, [RuII(η^6-p-cymene)Cl$_2$]$_2$ (0.142 g, 0.232 mmol) was added dropwise and allowed to reflux for 5 h. The solvent was evaporated under reduced pressure. The brown crude was washed two times with diethyl ether, yielding a deep brown solid. The product was dried in vacuum. Yield: 0.145 g (60%.) Anal. Calcd for $C_{21}H_{23}Cl_2N_3O_2Ru$: C, 48.38; H, 4.45; N, 8.06. Found C, 45.46; H, 4.51; N, 7.98. ^{1}H NMR (500 MHz, DMSO-d_6): δ 8.54 (s, 1H, Imi-H), 8.32 (s, 1H, –CH=N), 8.17 (s, 1H, Imi-H), 8.07 (d, 1H, J = 7.7 Hz, Ar–H), 8.02 (d, 1H, J = 6.8 Hz, Ar–H), 7.84 (d, 1H, J = 1.0 Hz, Ar–H), 7.74 (t, 1H, J = 7.9 Hz, Ar–H), 6.04 (d, 1H, J = 6.2 Hz, p-cym-H), 5.67 (d, 1H, J = 6.1 Hz, p-cym-H), 5.62 (d, 1H, J = 6.1 Hz, p-cym-H), 5.42 (d, 1H, J = 6.1 Hz, p-cym-H), 2.12 (s, 3H, p-cym-CH_3), 1.03 (d, 3H, J = 6.9 Hz, iPr–CH_3), 0.94 (d, 3H, J = 6.8 Hz, iPr–CH_3) (Figure S20). ^{13}C NMR (125 MHz, DMSO-d_6) δ 166.52, 155.56, 151.97, 146.37, 133.86, 131.87, 129.70, 129.51, 126.59, 124.24, 123.33, 104.09, 101.11, 85.12, 85.07, 83.18, 82.80, 30.41, 22.15, 20.98, 18.11 (Figure S21). UV-vis.: [CH_3OH, λ_{max}, nm(ε/dm^{3}mol^{-1}cm^{-1})]: 212 (6480), 320 (2800) (Figure S32). FT-IR (cm^{-1}): 3693, 2834, 1687, 1534, 1406, 1363, 1228, 1178, 1093, 745. ESI-HRMS (Methanol) m/z (calc): 486.0506 (486.0517) [$C_{21}H_{23}ClN_3O_2Ru^+$].

[(L4)Ru^{II}(η^6-p-cym)Cl]Cl (5). To a stirred solution of **L4** (0.1 g, 0.436 mmol) in methanol, [Ru^{II}(η^6-p-cymene)Cl$_2$]$_2$ (0.133 g, 0.218 mmol) was added dropwise and allowed to reflux for 6–7 h. The solvent was evaporated under reduced pressure. The deep orange crude was washed two times with diethyl ether, yielding an orange solid, with a yellow tinge. The product was dried in vacuum. Yield: 0.156 (67%). Anal. Calcd for $C_{22}H_{25}Cl_2N_3O_2Ru$: C, 49.35; H, 4.71; N, 7.85. Found C, 49.51; H, 4.76; N, 7.89. ^{1}H NMR (500 MHz, DMSO-d_6): δ 14.48 (br.s, 1H, Imi-NH), 8.55 (s, 1H, –CH=N), 8.34 (s, 1H, Imi-H), 8.18 (s, 1H, Imi-H), 8.09 (d, 1H, J = 7.8 Hz, Ar–H), 8.04 (d, 1H, J = 7.6 Hz, Ar–H), 7.85 (s, 1H, Ar–H), 7.76 (t, 1H, J = 7.9 Hz, Ar–H), 6.04 (d, 1H, J = 6.1 Hz, p-cym-H), 5.67 (d, 1H, J = 6.2 Hz, p-cym-H), 5.62 (d, 1H, J = 6.0 Hz, p-cym-H), 5.44 (d, 1H, J = 6.0 Hz, p-cym-H), 3.93 (s, 3H, –COOMe), 2.12 (s, 3H, p-cym-CH_3), 1.03 (d, 3H, J = 6.8 Hz, iPr–CH_3), 0.94 (d, 3H, J = 6.8 Hz, iPr–CH_3) (Figure S22). ^{13}C NMR (125 MHz, DMSO-d_6) δ 165.46, 155.67, 151.99, 142.26, 133.86, 130.57, 129.87, 129.31, 126.99, 124.17, 123.21, 104.23, 100.99, 85.14, 85.03, 83.20, 82.60, 52.47, 30.39, 22.11, 20.96, 18.04 (Figure S23). UV-vis.: [CH_3OH, λ_{max}, nm(ε/dm^{3}mol^{-1}cm^{-1})]: 212 (6480), 324 (2800) (Figure S32). FT-IR (cm^{-1}): 3513, 3375, 3230, 1693, 1562, 1472, 1431, 1362, 1210,

1106, 992, 747. ESI-HRMS (Methanol) m/z (calc): 500.0661 (500.0673) [$C_{22}H_{25}ClN_3O_2Ru^+$].

[(L4)Ru^{II}(η^6-p-cym)I]I (6). To a stirred solution of **L4** (0.1 g, 0.436 mmol) in methanol, [Ru^{II}(η^6-p-cymene)I_2]$_2$ (0.213 g, 0.218 mmol) was added dropwise and allowed to reflux for 7–8 h. The solvent was evaporated under reduced pressure. The orange crude was washed two times with diethyl ether, yielding a deep orange solid. The product was dried in vacuum. Yield: 0.185 g (59%). Anal. Calcd for $C_{22}H_{25}I_2N_3O_2Ru$: C, 36.79; H, 3.51; N, 5.85. Found C, 36.91; H, 3.48; N, 5.91. ^{1}H NMR (500 MHz, DMSO-d_6): δ 14.38 (br.s, 1H, Imi-NH), 8.49 (s, 1H, –CH=N), 8.41 (s, 1H, Imi-H), 8.15 (s, 1H, Imi-H), 8.11 (t, 2H, J = 6.9 Hz, Ar–H), 7.86 (s, 1H, Ar–H), 7.75 (t, 1H, J = 7.9 Hz, Ar–H), 5.93 (d, 1H, J = 6.1 Hz, p-cym-H), 5.73 (d, 1H, J = 6.2 Hz, p-cym-H), 5.67 (d, 1H, J = 6.0 Hz, p-cym-H), 5.43 (d, 1H, J = 6.0 Hz, p-cym-H), 3.93 (s, 3H, –COOMe), 2.65 (m, 1H, p-cym-CH), 2.29 (s, 3H, p-cym-CH_3), 1.05 (d, 3H, J = 6.8 Hz, iPr–CH_3), 0.92 (d, 3H, J = 6.8 Hz, iPr–CH_3) (Figure S24). ^{13}C NMR (125 MHz, DMSO-d_6) δ 165.43, 155.34, 152.46, 145.90, 134.87, 130.54, 129.81, 129.47, 127.66, 124.62, 123.93, 106.46, 99.70, 86.11, 84.18, 82.70, 52.50, 30.94, 22.17, 20.93, 19.50 (Figure S25). UV-vis.: [CH_3OH, λ_{max}, nm(ε/$dm^3mol^{-1}cm^{-1}$)]: 220 (8280), 334 (2410) (Figure S32). FT-IR (cm^{-1}): 3700, 3575, 2981, 2925, 1687, 1410, 1272, 1241, 1182, 1078, 739. ESI-HRMS (Methanol) m/z (calc): 592.0019 (592.0030) [$C_{22}H_{25}IN_3O_2Ru^+$]-

[(L5)Ru^{II}(η^6-p-cym)Cl] (7). To a solution of **L5** (0.07 g, 0.274 mmol), dissolved in 10 mL of methanol, KOH (0.14 g, 0.260 mmol) and [Ru^{II}(η^6-p-cymene)Cl_2]$_2$ (0.083 g, 0.137 mmol), also dissolved in methanol were added subsequently. The whole reaction mixture was allowed to stir at 25 °C for 24 h under nitrogen atmosphere. The solvent was filtered, evaporated under reduced pressure and the resulting orange crude was extracted with dichloromethane. The dichloromethane layer was evaporated under reduced pressure and washed two times with chilled diethyl ether to obtain a reddish-brown crude. The crude was purified by means of column chromatography, packed with neutral alumina, using 0.1% methanol in dichloromethane as eluent. Product was isolated as a reddish-orange powder. Yield: 0.081 g (57%). Anal. Calcd for $C_{25}H_{26}ClNO_3Ru$: C, 57.19; H, 4.99; N, 2.67. Found C, 56.81; H, 4.95; N, 2.72. ^{1}H NMR (400 MHz, $CDCl_3$): δ 10.82 (s, 1H, –CH=N), 8.01 (d, 1H, J = 2.5 Hz, Sal-H), 7.95 (dd, 1H, Sal-H), 7.73 (s, 1H, Ar–H), 7.24 (m, 1H, Sal-H), 7.07 (d, 1H, J = 8.6 Hz, Ar–H), 7.02 (d, 1H, J = 8.6 Hz, Ar–H), 6.97 (dd, 1H, Ar–H), 6.46 (t, 1H, J = 7.1 Hz, Sal-H), 5.37 (d, 1H, J = 6.1 Hz, p-cym-H), 5.30 (d, 1H, J = 6.1 Hz, p-cym-H), 5.03 (d, 1H, J = 5.8 Hz, p-cym-H), 4.31 (d, 1H, J = 5.8 Hz, p-cym-H), 4.02 (s, 3H, -OMe), 2.68 (m, 1H, p-cym-CH), 2.14 (s, 3H, p-cym-CH_3), 1.20 (d, 3H, J = 6.9 Hz, iPr–CH_3), 1.13 (d, 3H, J = 6.9 Hz, iPr–CH_3) (Figure S26). ^{13}C NMR (125 MHz, $CDCl_3$) δ 166.56, 165.69, 164.81, 158.62, 136.01, 135.60, 131.04, 129.65, 129.24, 128.18, 123.77, 122.97, 118.22, 114.57, 107.01,102.00, 97.96, 86.62, 83.76, 83.68, 80.07, 52.67, 30.55, 22.91, 21.74, 18.58 (Figure S27). UV-vis.: [CH_3OH, λ_{max}, nm(ε/$dm^3mol^{-1}cm^{-1}$)]: 222 (53910), 292 (15740), 412 (5380) (Figure S33). FT-IR (cm^{-1}): 2829, 2018, 1691, 1576, 1501, 1419, 1269, 745. ESI-HRMS (Methanol) m/z (calc): 490.0952 (490.0958) [$C_{25}H_{26}NO_3Ru^+$].

[(L6)Ru^{II}(η^6-p-cym)Cl] (8). To a solution of **L6** (0.08 g, 0.305 mmol), dissolved in 10 mL of methanol, KOH (0.14 g, 0.262 mmol) and [Ru^{II}(η^6-p-cymene)Cl_2]$_2$ (0.081 g, 0.131 mmol), also dissolved in methanol were added subsequently. The whole reaction mixture was allowed to stir at 25 °C for 24 h under nitrogen atmosphere. The solvent was filtered, evaporated under reduced pressure and the resulting deep orange crude was extracted with dichloromethane. The dichloromethane layer was evaporated under reduced pressure and washed two times with chilled diethyl ether to obtain a reddish-brown crude. The crude was purified by means of column chromatography, packed with neutral alumina, using 0.1% methanol in dichloromethane as eluent. Product was isolated as a reddish-orange powder. Yield: 0.083 g (55%). Anal. Calcd for $C_{29}H_{28}ClNO_3Ru$: C, 60.57; H, 4.91; N, 2.44. Found C, 60.39; H, 4.87; N, 2.48. ^{1}H NMR (400 MHz, $CDCl_3$): δ 8.57 (s, 1H, –CH=N), 8.18 (s, 1H, Ar–H), 8.06 (m, 2H, Naph-H), 7.69 (d, 1H, J = 8.8 Hz, Naph -H), 7.64 (d, 1H, J = 9.3 Hz, Naph -H), 7.57 (m, 2H, Ar–H and Naph -H), 7.34 (m, 1H, Naph-H), 7.18 (m, 2H, Ar–H), 5.41 (d, 1H, J = 6.0 Hz, p-cym-H), 5.30 (d, 1H, J = 6.2 Hz, p-cym-H), 5.02 (d, 1H, J = 5.7 Hz, p-cym-H), 4.25 (d, 1H, J = 5.5 Hz, p-cym-H), 3.99 (s, 3H, –OMe), 2.67 (m, 1H, p-cym-CH), 2.14 (s, 3H, p-cym-CH_3), 1.19 (d, 3H, J = 6.9 Hz, iPr–CH_3), 1.13 (d, 3H, J = 6.9 Hz, iPr–CH_3) (Figure S28). ^{13}C NMR (125 MHz, $CDCl_3$) δ 166.65, 166.58, 159.69, 158.23, 136.37, 134.93, 131.09, 129.99, 129.22, 129.04, 127.93, 127.58, 126.81, 125.52, 124.41, 122.21, 118.74, 108.44, 101.94, 97.93, 86.65, 84.49, 83.98, 80.28, 52.65, 30.61, 22.91, 21.72, 18.64 (Figure S29). UV-vis.: [CH_3OH, λ_{max}, nm(ε/$dm^3mol^{-1}cm^{-1}$)]: 251 (39720), 325 (13900), 439 (4470) (Figure S33). FT-IR (cm^{-1}): 2880, 2058, 1696, 1588, 1416, 1270, 739. ESI-HRMS (Methanol) m/z (calc): 540.1109 (540.1107) [$C_{29}H_{28}NO_3Ru^+$].

[(L7)Ru^{II}(η^6-p-cym)Cl] (9). To a solution of **L7** (0.08 g, 0.285 mmol), dissolved in 10 mL of methanol, KOH (0.16 g, 0.280 mmol) and [Ru^{II}(η^6-p-cymene)Cl_2]$_2$ (0.085 g, 0.14 mmol), also dissolved in methanol were added subsequently. The whole reaction mixture was allowed to stir at 25 °C for 24 h under nitrogen atmosphere. The solvent was filtered, evaporated under reduced pressure and the resulting orange crude was extracted with dichloromethane. The dichloromethane layer was evaporated under reduced pressure and washed two times with chilled diethyl ether to obtain a yellowish-orange crude. The crude was purified by means of column chromatography, packed with neutral alumina, using 0.1% methanol in dichloromethane as eluent. Product was isolated as a deep yellow orange powder. Yield: 0.085 g (55%). Anal. Calcd for $C_{26}H_{28}ClNO_4Ru$: C, 56.26; H, 5.09; N, 2.52. Found C, 56.43; H, 5.06; N, 2.58. ^{1}H NMR (400 MHz, $CDCl_3$): δ 8.13 (s, 1H, Ar–H), 8.10 (dd, 1H, Ar–H), 8.03 (m, 1H, Ar–H), 7.75 (s, 1H, –CH=N), 7.54 (t, 1H, J = 7.8 Hz, Ar–H), 6.76 (dd, 1H, Van-H), 6.61 (dd, 1H, Van-H), 6.39 (t, 1H, J = 7.8 Hz, Van-H), 5.37 (d, 1H, J = 6.0 Hz, p-cym-H), 5.30 (d, 1H, J = 6.0 Hz, p-cym-H), 5.04 (d, 1H, J = 5.9 Hz, p-cym-H), 4.29 (d, 1H, J = 5.7 Hz, p-cym-H), 3.99 (s, 3H, Ar-OMe), 3.83 (s, 3H, Van-OMe), 2.68 (m, 1H, p-cym-CH), 2.10 (s, 3H, p-cym-CH_3), 1.18 (d, 3H, J = 7.1 Hz, iPr–CH_3), 1.12 (d, 3H, J = 7.0 Hz, iPr–CH_3) (Figure S30). ^{13}C NMR (125 MHz, $CDCl_3$) δ 166.34, 161.45 164.45, 158.46, 157.10, 152.66, 130.84, 129.63, 129.04, 127.97, 126.90, 123.69, 117.89, 115.37, 113.31, 102.10, 97.68, 86.26, 83.68, 83.45, 79.97, 56.19, 52,49, 30.30, 22.77, 21.52, 18.33 (Figure S31). UV-vis.: [CH_3OH, λ_{max}, nm(ε/$dm^3mol^{-1}cm^{-1}$)]: 237 (26380), 284 (9220), 430 (2200) (Figure S33). FT-IR (cm^{-1}): 2901, 1692, 1567, 1501, 1423, 1208, 739. ESI-HRMS (Methanol) m/z (calc): 520.1064 (520.1056) [$C_{26}H_{28}NO_4Ru^+$].

X-Ray Crystallography. Good quality single crystals suitable for X-ray diffraction were obtained by layering dichloromethane solutions of the isolated complexes (**2** and **5**) with hexane. Single crystals were mounted using loops on the goniometer head of a SuperNova, Dual, Cu at zero, Eos diffractometer (Agilent) equipped with graphite monochromated Cu–Kα radiation (1.5406 Å) and data collected at 100 K. An empirical multi-scan absorption correction was performed using SADABS. The structures were solved by direct methods and all non-hydrogen atoms were refined anisotropically by full matrix least-squares on F^2. A few important crystallographic parameters are summarized in Table 1 and Table S1. The hydrogen atoms were calculated and fixed using riding model in SHELXL-97 after hybridization of all non-hydrogen atoms. The CCDC deposition numbers are 2088610 and 2088611 respectively for **2** and **5**.

Stability studies in aqueous buffer solution. The complexes were dissolved in a mixture of DMSO-d_6 and 10 mM phosphate buffer (pD = 7.4) containing 4 mM NaCl (3:7 v/v) and the spectra were recorded by ^{1}H-NMR at 25 °C at different time intervals. The stabilities of complexes **3** and **6** were also determined by dissolving

the respective complexes in 600 μL of 3:7 (v/v) DMSO-d_6:10 mM phosphate buffer (pD = 7.4) containing 130 mM NaCl at 25 °C. The ^{1}H-NMR spectra were recorded at various time intervals up to 24 h.

Binding studies with model nucleobase 9-ethylguanine (9-EtG). One molar equivalent of the complexes was co-incubated with 2 molar equivalents of 9-EtG in a 3:7 v/v DMSO-d_6: 10 mM phosphate buffer (pD = 7.4) containing 4 mM NaCl and the spectra were recorded at 25 °C by ^{1}H-NMR for 24 h at different time intervals. The ESI-MS studies of complexes **5** and **6** were done using a 1:2 ratio of the complexes w.r.t 9-EtG in a 2:8 (v/v) mixture of methanol and 10 mM phosphate buffer (pH = 7.4) containing 4 mM NaCl at 25 °C. The data were analyzed and plotted using Bruker Daltonics software.

Distribution coefficient distribution determination. The distribution coefficient (log D) was determined using the traditional shake-flask method using octanol-10 mM phosphate buffer solution containing 4 mM NaCl (pH = 7.4). After pre-equilibration of octanol and aqueous phosphate buffer solutions (2 mL each) overnight, **1**–**9** (1 mg each) were added and shaken continuously (150 rpm) at 37 °C for 6 h on a BOD incubator. The tubes were then centrifuged, and aliquots of the octanol and aqueous buffer layers were pipetted out separately. Absorbances were measured, with necessary dilutions, by means of UV-Visible spectroscopy. Each set was performed in triplicate. Concentration in each layer was determined from the respective molar extinction coefficient values and the corresponding distribution coefficient (log D) was calculated.

Cell lines and culture condition. Triple negative human metastatic breast adenocarcinoma (MDA-MB-231) was bought from NCCS, Pune, India. Cell lines were maintained in the logarithmic phase at 37 °C in a 5% carbon dioxide atmosphere using a suitable culture media, 10% fetal bovine serum (GIBCO) and 1% antibiotic-antimycotic solution. The culture medium used was a 1:1 mixture of Dulbecco's modified Eagle's medium (DMEM) with Ham's F12 nutrient mixture, i.e. (DMEM/F12) medium.

Cell viability assay. The growth inhibitory effect towards MDA-MB-231 tumor cell line was evaluated with the help of MTT assay. In brief, 6×10^3 cells per well, were seeded in 96-well micro-plates in media (200 μL) and incubated at 37 °C in a 5% carbon dioxide atmosphere. After 24 h, media was renewed with a fresh one (200 μL). Stock solutions of **1**–**9** in DMSO-media mixture were made immediately prior to drug dilution. Various concentrations of solution were prepared from the stock solution diluted with the same culture media within 5 min and added in triplicate to attain appropriate concentrations in the respective wells. The final DMSO concentration in well did not exceed 0.2%. Same DMSO percentage used in all cell-based studies. Upon completion of 72 h incubation with the compounds, new media (200 μL) added to each well and the old drug-containing media removed. Then 20 μL of a 1 mg mL^{-1} MTT in 1×PBS (pH = 7.2) added followed by 3 h of incubation at 37 °C. Finally, the media removed and the resulting formazan crystals dissolved in spectroscopy grade DMSO (200 μL). Analysis of the growth inhibition of the cells done by comparing the absorbance (570 nm) of the drug-treated wells with respect to the untreated ones using either a BIOTEK ELx800 or a SpectraMax M2e plate reader. IC_{50} values (drug concentrations that is responsible for 50% cell growth inhibition) were calculated by fitting non-linear curves (four-parameter fitting) in GraphPad Prism 5, with variable slope model. The data plotted as cell viability (%) *vs.* log of drug concentration in μM. Each independent experiment was carried out in triplicate.

Cell cycle arrest. 1×10^5 MDA-MB-231 cells were cultured in 35 mm 6-well plates with 2 mL of DMEM-F12, under previously described culturing conditions. Once the cells attained confluency of 60–70% the old culture medium was removed and replenished with a fresh medium. 3 and 2 μM concentrations of **5**, 2 and 1 μM of **6**, 5 and 7 μM concentrations of **8**, were added to the respective wells and incubated under the same conditions as described above. The cells were exposed to complexes **5** and **6** for 24 h but 18 h in case of **8**, due to their activity differences. The cells were harvested by trypsinization, centrifuged and washed twice with cold 1 × PBS (pH = 7.2). Cells were resuspended in 600 μL of cold 1×PBS and fixed with 1400 μL ethanol overnight at −20 °C. DNA staining was done by resuspending the cell pellets in 1× PBS solution containing PI (55 μg mL^{-1}) and RNaseA (100 μg mL^{-1}). Cell suspensions were gently mixed and incubated at 37 °C for 0.5 h in a dry bath. The samples were analyzed in BD Biosciences FACS Calibur flow cytometer.

Apoptosis assay. Apoptosis was detected by PE-Annexin V/ 7-AAD dual staining apoptosis kit (BD PharmingenTM, catalog no. 559763) by means of flow cytometry, as per manufacturers' protocol. 1×10^5 MDA-MB-231 cells were seeded in 100 mm sterile tissue culture petri dishes using 6 mL of DMEM–F12 media. Then the cells were incubated at 37 °C in a 5% CO_2 atmosphere for 48 h. After incubation, the media was changed and treated with two different concentrations of **8** (5 and 7 μM) for 18 h. The treated and untreated cells were harvested by cold 1×PBS containing 0.1 mM EDTA and then washed twice with cold 1×PBS. Cells were resuspended in Annexin V binding buffer. Annexin V and 7-AAD were incubated for 15 minutes in the dark at 25 °C. Data were recorded and analyzed in a BD Biosciences FACS Calibur flow cytometer within 30 minutes of sample preparation.

Author Contributions

The project was designed by Arindam Mukherjee. Arpan Mukherjee performed the synthesis, characterization, NMR and ESI-MS for solution stability, 9-EtG reactivity, lipophilicity. TSK performed all the cytotoxicity data, cell cycle and apoptosis. AC helped in some of the cytotoxicity data. SR verified few cytotoxicity data and coordinated the manuscript writing. AM supervised the overall work. All authors have approved the final version of the manuscript.

Supporting Information

The supporting information contains ^{1}H-NMR and ^{13}C-NMR of ligands (**L1** to **L7**; Figures S1–S13) and complexes (**1**–**9**; Figures S14–S31), UV-Visible spectra of complexes (**1**–**9**); Figures S32–S33), Selected parameters in crystallography (Table S1), time-dependent ^{1}H-NMR studies of complexes **1**–**9** for stability and halide exchange (Figures S34–S43), time-dependent ^{1}H-NMR studies of 9-EtG binding to complexes **2**,**3**,**5** & **6** by ^{1}H-NMR and ESI-HRMS (Figures S44–S52), Representative MTT assay plots (Figures S53–S54), cell cycle arrest and apoptosis (Figures S55–S58).

Acknowledgements

We earnestly acknowledge SERB, Government of India, via EMR/2017/002324 for funding this work. We also thank IISER Kolkata

for infra-structural and financial support. A.M. thanks CSIR, and T.S.K. thanks IISER–K for their research fellowships. We are thankful to S.A. for the oxaliplatin data. We also thank Mr. Tamal Ghosh for helping us in flow cytometry analysis studies.

Conflict of Interest

The authors declare no conflict of interest.

Keywords: Ru^{II}-p-cymene · cytotoxicity · *N,N* and *N,O* coordination · solution stability · 3-aminobenzoate

[1] E. Wong, C. M. Giandomenico, *Chem. Rev.* **1999**, *99*, 2451–2466.
[2] L. Zeng, P. Gupta, Y. Chen, E. Wang, L. Ji, H. Chao, Z.-S. Chen, *Chem. Soc. Rev.* **2017**, *46*, 5771–5804.
[3] S. M. Meier-Menches, C. Gerner, W. Berger, C. G. Hartinger, B. K. Keppler, *Chem. Soc. Rev.* **2018**, *47*, 909–928.
[4] S. Thota, D. A. Rodrigues, D. C. Crans, E. J. Barreiro, *J. Med. Chem.* **2018**, *61*, 5805–5821.
[5] A. R. Timerbaev, *Metallomics* **2009**, *1*, 193–198.
[6] C. R. Chitambar, *Future Med. Chem.* **2012**, *4*, 1257–1272.
[7] C. R. Chitambar, M. M. Al-Gizawiy, H. S. Alhajala, K. R. Pechman, J. P. Wereley, R. Wujek, P. A. Clark, J. S. Kuo, W. E. Antholine, K. M. Schmainda, *Mol. Cancer Ther.* **2018**, *17*, 1240–1250.
[8] R. Trondl, P. Heffeter, C. R. Kowol, M. A. Jakupec, W. Berger, B. K. Keppler, *Chem. Sci.* **2014**, *5*, 2925–2932.
[9] E. Alessio, L. Messori, *Molecules* **2019**, *24*, 1995.
[10] S. Monro, K. L. Colon, H. Yin, J. Roque, P. Konda, S. Gujar, R. P. Thummel, L. Lilge, C. G. Cameron, S. A. McFarland, *Chem. Rev.* **2019**, *119*, 797–828.
[11] J. Liu, H. Lai, Z. Xiong, B. Chen, T. Chen, *Chem. Commun.* **2019**, *55*, 9904–9914.
[12] Z. Tian, J. Li, S. Zhang, Z. Xu, Y. Yang, D. Kong, H. Zhang, X. Ge, J. Zhang, Z. Liu, *Inorg. Chem.* **2018**, *57*, 10498–10502.
[13] J. Zhao, W. Li, S. Gou, S. Li, S. Lin, Q. Wei, G. Xu, *Inorg. Chem.* **2018**, *57*, 8396–8403.
[14] O. A. Lenis-Rojas, M. P. Robalo, A. I. Tomaz, A. Carvalho, A. R. Fernandes, F. Marques, M. Folgueira, J. Yanez, D. Vazquez-Garcia, M. Lopez Torres, A. Fernandez, J. J. Fernandez, *Inorg. Chem.* **2018**, *57*, 13150–13166.
[15] S. J. Allison, D. Cooke, F. S. Davidson, P. I. P. Elliott, R. A. Faulkner, H. B. S. Griffiths, O. J. Harper, O. Hussain, P. J. Owen-Lynch, R. M. Phillips, C. R. Rice, S. L. Shepherd, R. T. Wheelhouse, *Angew. Chem. Int. Ed.* **2018**, *57*, 9799–9804; *Angew. Chem.* **2018**, *130*, 9947–9952.
[16] J. Zhao, S. Li, X. Wang, G. Xu, S. Gou, *Inorg. Chem.* **2019**, *58*, 2208–2217.
[17] C. Zhang, R. Guan, X. Liao, C. Ouyang, T. W. Rees, J. Liu, Y. Chen, L. Ji, H. Chao, *Chem. Commun.* **2019**, *55*, 12547–12550.
[18] D. Wernitznig, K. Kiakos, G. Del Favero, N. Harrer, H. Machat, A. Osswald, M. A. Jakupec, A. Wernitznig, W. Sommergruber, B. K. Keppler, *Metallomics* **2019**, *11*, 1044–1048.
[19] A. Mitrovic, J. Kljun, I. Sosic, M. Ursic, A. Meden, S. Gobec, J. Kos, I. Turel, *Inorg. Chem.* **2019**, *58*, 12334–12347.
[20] J. McCain, K. L. Colon, P. C. Barrett, S. M. A. Monro, T. Sainuddin, J. Roque III, M. Pinto, H. Yin, C. G. Cameron, S. A. McFarland, *Inorg. Chem.* **2019**, *58*, 10778–10790.
[21] C. Liu, R. Zhang, W. Zhang, J. Liu, Y.-L. Wang, Z. Du, B. Song, Z. P. Xu, J. Yuan, *J. Am. Chem. Soc.* **2019**, *141*, 8462–8472.
[22] J. Kladnik, J. Kljun, H. Burmeister, I. Ott, I. Romero-Canelon, I. Turel, *Chem. Eur. J.* **2019**, *25*, 14169–14182.
[23] Y. Lin, J. Wang, W. Zheng, Q. Luo, K. Wu, J. Du, Y. Zhao, F. Wang, *Metallomics* **2019**, *11*, 546–555.
[24] L. Corte-Real, B. Karas, A. R. Bras, A. Pilon, F. Avecilla, F. Marques, A. Preto, B. T. Buckley, K. R. Cooper, C. Doherty, M. H. Garcia, A. Valente, *Inorg. Chem.* **2019**, *58*, 9135–9149.
[25] F. J. Ballester, E. Ortega, V. Porto, H. Kostrhunova, N. Davila-Ferreira, D. Bautista, V. Brabec, F. Dominguez, M. D. Santana, J. Ruiz, *Chem. Commun.* **2019**, *55*, 1140–1143.
[26] R. Pettinari, F. Marchetti, C. Di Nicola, C. Pettinari, A. Galindo, R. Petrelli, L. Cappellacci, M. Cuccioloni, L. Bonfili, A. M. Eleuteri, M. F. C. Guedes da Silva, A. J. L. Pombeiro, *Inorg. Chem.* **2018**, *57*, 14123–14133.
[27] F. Martinez-Pena, S. Infante-Tadeo, A. Habtemariam, A. M. Pizarro, *Inorg. Chem.* **2018**, *57*, 5657–5668.
[28] J. Li, M. Tian, Z. Tian, S. Zhang, C. Yan, C. Shao, Z. Liu, *Inorg. Chem.* **2018**, *57*, 1705–1716.
[29] J. Li, L. Guo, Z. Tian, S. Zhang, Z. Xu, Y. Han, R. Li, Y. Li, Z. Liu, *Inorg. Chem.* **2018**, *57*, 13552–13563.
[30] N. Y. S. Lam, D. Truong, H. Burmeister, M. V. Babak, H. U. Holtkamp, S. Movassaghi, D. M. Ayine-Tora, A. Zafar, M. Kubanik, L. Oehninger, T. Sohnel, J. Reynisson, S. M. F. Jamieson, C. Gaiddon, I. Ott, C. G. Hartinger, *Inorg. Chem.* **2018**, *57*, 14427–14434.
[31] M. M. Haghdoost, J. Guard, G. Golbaghi, A. Castonguay, *Inorg. Chem.* **2018**, *57*, 7558–7567.
[32] M. J. Chow, M. V. Babak, K. W. Tan, M. C. Cheong, G. Pastorin, C. Gaiddon, W. H. Ang, *Mol. Pharmaceutics* **2018**, *15*, 3020–3031.
[33] R. F. Brissos, P. Clavero, A. Gallen, A. Grabulosa, L. A. Barrios, A. B. Caballero, L. Korrodi-Gregorio, R. Perez-Tomas, G. Muller, V. Soto-Cerrato, P. Gamez, *Inorg. Chem.* **2018**, *57*, 14786–14797.
[34] W. Ma, L. Guo, Z. Tian, S. Zhang, X. He, J. Li, Y. Yang, Z. Liu, *Dalton Trans.* **2019**, *48*, 4788–4793.
[35] F. Chen, I. Romero-Canelon, J. J. Soldevila-Barreda, J.-I. Song, J. P. C. Coverdale, G. J. Clarkson, J. Kasparkova, A. Habtemariam, M. Wills, V. Brabec, P. J. Sadler, *Organometallics* **2018**, *37*, 1555–1566.
[36] A. K. Renfrew, *Metallomics* **2014**, *6*, 1324–1335.
[37] P. Schluga, G. Hartinger Christian, A. Egger, E. Reisner, M. Galanski, A. Jakupec Michael, K. Keppler Bernhard, *Dalton Trans.* **2006**, 1796–1802.
[38] X. Wang, X. Wang, S. Jin, N. Muhammad, Z. Guo, *Chem. Rev.* **2019**, *119*, 1138–1192.
[39] H. Chen, J. A. Parkinson, S. Parsons, R. A. Coxall, R. O. Gould, P. J. Sadler, *J. Am. Chem. Soc.* **2002**, *124*, 3064–3082.
[40] A. F. A. Peacock, A. Habtemariam, R. Fernandez, V. Walland, F. P. A. Fabbiani, S. Parsons, R. E. Aird, D. I. Jodrell, P. J. Sadler, *J. Am. Chem. Soc.* **2006**, *128*, 1739–1748.
[41] F. Wang, A. Habtemariam, E. P. L. van der Geer, R. Fernandez, M. Melchart, R. J. Deeth, R. Aird, S. Guichard, F. P. A. Fabbiani, P. Lozano-Casal, I. D. H. Oswald, D. I. Jodrell, S. Parsons, P. J. Sadler, *Proc. Natl. Acad. Sci. USA* **2005**, *102*, 18269–18274.
[42] A. F. A. Peacock, P. J. Sadler, *Chem. Asian J.* **2008**, *3*, 1890–1899.
[43] T. Bugarcic, A. Habtemariam, J. Stepankova, P. Heringova, J. Kasparkova, R. J. Deeth, R. D. L. Johnstone, A. Prescimone, A. Parkin, S. Parsons, V. Brabec, P. J. Sadler, *Inorg. Chem.* **2008**, *47*, 11470–11486.
[44] Y. K. Yan, M. Melchart, A. Habtemariam, P. J. Sadler, *Chem. Commun.* **2005**, 4764–4776.
[45] A. Habtemariam, M. Melchart, R. Fernandez, S. Parsons, I. D. H. Oswald, A. Parkin, F. P. A. Fabbiani, J. E. Davidson, A. Dawson, R. E. Aird, D. I. Jodrell, P. J. Sadler, *J. Med. Chem.* **2006**, *49*, 6858–6868.
[46] L. Corte-Real, R. G. Teixeira, P. Girio, E. Comsa, A. Moreno, R. Nasr, H. Baubichon-Cortay, F. Avecilla, F. Marques, M. P. Robalo, P. Mendes, J. P. P. Ramalho, M. H. Garcia, P. Falson, A. Valente, *Inorg. Chem.* **2018**, *57*, 4629–4639.
[47] E. S. Antonarakis, A. Emadi, *Cancer Chemother. Pharmacol.* **2010**, *66*, 1–9.
[48] R. E. Morris, R. E. Aird, P. d S Murdoch, H. Chen, J. Cummings, N. D. Hughes, S. Parsons, A. Parkin, G. Boyd, D. I. Jodrell, P. J. Sadler, *J. Med. Chem.* **2001**, *44*, 3616–3621.
[49] I. Romero-Canelon, A. M. Pizarro, A. Habtemariam, P. J. Sadler, *Metallomics* **2012**, *4*, 1271–1279.
[50] I. Romero-Canelon, L. Salassa, P. J. Sadler, *J. Med. Chem.* **2013**, *56*, 1291–1300.
[51] D. N. Pantic, S. Arandjelovic, S. Radulovic, A. Roller, V. B. Arion, S. Grguric-Sipka, *J. Organomet. Chem.* **2016**, *819*, 61–68.
[52] R. M. Lord, S. J. Allison, K. Rafferty, L. Ghandhi, C. M. Pask, P. C. McGowan, *Dalton Trans.* **2016**, *45*, 13196–13203.
[53] S. Bhattacharyya, K. Purkait, A. Mukherjee, *Dalton Trans.* **2017**, *46*, 8539–8554.
[54] A. Mukherjee, S. Acharya, K. Purkait, K. Chakraborty, A. Bhattacharjee, A. Mukherjee, *Inorg. Chem.* **2020**, *59*, 6581–6594.
[55] K. Purkait, Ruturaj, A. Mukherjee, A. Gupta, *Inorg. Chem.* **2019**, *58*, 15659–15670.
[56] J. Ferlay, I. Soerjomataram, R. Dikshit, S. Eser, C. Mathers, M. Rebelo, D. M. Parkin, D. Forman, F. Bray, *Int. J. Cancer* **2015**, *136*, E359-E386.
[57] H. A. Wahba, H. A. El-Hadaad, *Cancer Biol. Med.* **2015**, *12*, 106–116.
[58] L. Biancalana, S. Zacchini, N. Ferri, M. G. Lupo, G. Pampaloni, F. Marchetti, *Dalton Trans.* **2017**, *46*, 16589–16604.
[59] N. Wambang, N. Schifano-Faux, A. Martoriati, N. Henry, B. Baldeyrou, C. Bal-Mahieu, T. Bousquet, S. Pellegrini, S. Meignan, K. Cailliau, J.-F.

Goossens, J.-F. Bodart, P. T. Ndifon, L. Pelinski, *Organometallics* **2016**, *35*, 2868–2872.
[60] L. Boubakri, A. Chakchouk-Mtibaa, A. S. Al-Ayed, L. Mansour, N. Abutaha, A. H. Harrath, L. Mellouli, I. Ozdemir, S. Yasar, N. Hamdi, *RSC Adv.* **2019**, *9*, 34406–34420.
[61] I. Slimani, A. Chakchouk-Mtibaa, L. Mansour, L. Mellouli, I. Ozdemir, N. Gurbuzd, N. Hamdi, *New J. Chem.* **2020**, *44*, 5309–5323.
[62] A. Savic, N. Gligorijevic, S. Arandjelovic, B. Dojcinovic, A. M. Kaczmarek, S. Radulovic, R. Van Deun, K. Van Hecke, *J. Inorg. Biochem.* **2020**, *202*, 110869.
[63] B. N. Cunha, L. Luna-Dulcey, A. M. Plutin, R. G. Silveira, J. Honorato, R. R. Cairo, T. D. de Oliveira, M. R. Cominetti, E. E. Castellano, A. A. Batista, *Inorg. Chem.* **2020**, *59*, 5072–5085.
[64] J. Pracharova, V. Novohradsky, H. Kostrhunova, P. Starha, Z. Travnicek, J. Kasparkova, V. Brabec, *Dalton Trans.* **2018**, *47*, 12197–12208.
[65] S. Acharya, S. Ghosh, M. Maji, A. R. U. Parambil, S. Singh, A. Mukherjee, *Chem. Commun.* **2020**, *56*, 5421–5424.
[66] A. Sarkar, S. Acharya, K. Khushvant, K. Purkait, A. Mukherjee, *Dalton Trans.* **2019**, *48*, 7187–7197.
[67] S. Acharya, M. Maji, Ruturaj, K. Purkait, A. Gupta, A. Mukherjee, *Inorg. Chem.* **2019**, *58*, 9213–9224.
[68] J. M. Gichumbi, H. B. Friedrich, B. Omondi, *J. Coord. Chem.* **2019**, *72*, 135–147.
[69] K. Purkait, S. Chatterjee, S. Karmakar, A. Mukherjee, *Dalton Trans.* **2016**, *45*, 8541–8555.
[70] K. Purkait, S. Karmakar, S. Bhattacharyya, S. Chatterjee, S. K. Dey, A. Mukherjee, *Dalton Trans.* **2015**, *44*, 5969–5973.
[71] M. Schmidlehner, V. Pichler, A. Roller, M. A. Jakupec, W. Kandioller, B. K. Keppler, *J. Organomet. Chem.* **2015**, *782*, 69–76.
[72] M. Kubanik, H. Holtkamp, T. Sohnel, S. M. F. Jamieson, C. G. Hartinger, *Organometallics* **2015**, *34*, 5658–5668.
[73] J. Ruiz, V. Rodriguez, N. Cutillas, A. Espinosa, M. J. Hannon, *Inorg. Chem.* **2011**, *50*, 9164–9171.
[74] H. Zhang, L. Guo, Z. Tian, M. Tian, S. Zhang, Z. Xu, P. Gong, X. Zheng, J. Zhao, Z. Liu, *Chem. Commun.* **2018**, *54*, 4421–4424.
[75] S. Acharya, M. Maji, M. P. Chakraborty, I. Bhattacharya, R. Das, A. Gupta, A. Mukherjee, *Inorg. Chem.* **2021**, *60*, 3418–3430.
[76] J. Pitchaimani, M. R. Charan Raja, S. Sujatha, S. Kar Mahapatra, D. Moon, S. P. Anthony, V. Madhu, *RSC Adv.* **2016**, *6*, 90982–90992.
[77] M. Frik, A. Martinez, B. T. Elie, O. Gonzalo, D. Ramirez de Mingo, M. Sanau, R. Sanchez-Delgado, T. Sadhukha, S. Prabha, J. W. Ramos, I. Marzo, M. Contel, *J. Med. Chem.* **2014**, *57*, 9995–10012.
[78] J. Massague, *Nature* **2004**, *432*, 298–306.
[79] D. D. Perrin, W. L. F. Armarego, *Purification of Laboratory Chemicals. 3rd Ed*, Butterworth-Heinemann Ltd. **1988**.
[80] M. A. Bennett, T. N. Huang, T. W. Matheson, A. K. Smith, *Inorg. Synth.* **1982**, *21*, 74–78.

Manuscript received: August 9, 2021
Revised manuscript received: September 17, 2021
Accepted manuscript online: September 22, 2021
Version of record online: October 11, 2021